SIAM J. APPL. MATH.
Vol. 84, No. 4, pp. 1580–1608

UNIFORM ASYMPTOTIC APPROXIMATIONS FOR THE PHASE PLANE TRAJECTORIES OF THE SIR MODEL WITH VITAL DYNAMICS*

TODD L. PARSONS† AND DAVID J. D. EARN‡

Abstract. We derive accurate, closed-form analytical approximations for the phase-plane trajectories of the standard susceptible-infectious-removed (SIR) epidemic model, including host births and deaths, giving a complete description of the transient dynamics. Our approximations for the SIR ordinary differential equations also allow us to provide convenient, accurate analytical approximations for the associated Poincaré map, and the minimum and maximum susceptible and infectious host densities in each epidemic wave. Our analysis involves matching asymptotic expansions across branch cuts of the Lambert W function.

Key words. epidemics, SIR model, matched asymptotics, Poincaré map

MSC codes. 34E05, 34E13, 37N25, 92D30

DOI. 10.1137/23M1576050

1. Introduction.

Infectious disease transmission dynamics have been modeled with a susceptible-infectious-removed (SIR) compartmental framework since the early 20th century [19, 3]. What has become the standard SIR ordinary differential equation (ODE) model ((1.1) below) was first published by Kermack and McKendrick in 1927 [13] (hereafter KM). The SIR model, with and without vital dynamics (host births and deaths), and the simpler susceptible-infectious-susceptible (SIS) model, together have been called "the three most basic epidemiological models for microparasitic infections" [11].

The SIS model can easily be solved exactly [11]. In contrast, an exact solution for the time course of the state variables in the standard SIR ODEs has never been found, though KM did find an approximate analytical solution that is reasonably accurate for weakly transmissible diseases and that has often been used to obtain (usually qualitative) insights (e.g., [4, 26, 22]).

If we ignore the recruitment of new susceptible individuals—whether they result from births, immigration, or decay of immunity—then the SIR ODEs can be solved exactly in the susceptible-infectious phase plane [11]. No such exact analytical solution in the phase plane is available for the more realistic situation in which susceptible recruitment is not negligible.

In this paper, we use multiple scale and singular perturbation methods [24, 14] to obtain accurate analytical approximations to the phase-plane trajectories of the standard SIR ODEs with vital dynamics. A natural small parameter is the infectious period relative to host lifetime (denoted ε), but we find that substantially simpler

*Received by the editors May 30, 2023; accepted for publication (in revised form) February 15, 2024; published electronically July 22, 2024.
https://doi.org/10.1137/23M1576050
Funding: This work was partially supported by the CNRS IEA grant "Structured Populations, Epidemics & Control Strategies (SPECS)." The work of the second author was also supported by an NSERC Discovery Grant.
†LPSM, Sorbonne Université, CNRS UMR, 8001, Paris, 75005, France (todd.parsons@upmc.fr).
‡Department of Mathematics and Statistics, McMaster University, Hamilton L8S 4K1, ON, Canada (earn@math.mcmaster.ca).

expressions are obtained by expanding in the (even smaller) parameter[1] $\epsilon = \varepsilon/\mathcal{R}_0$, where $\mathcal{R}_0$ is the basic reproduction number.

Our interest in approximating the phase-plane solutions of the SIR ODEs was motivated by a problem in stochastic epidemic theory, namely estimating the probability of persistence of a pathogen after an initial epidemic in a naïve population. Our solution to that problem [25] depends on an analytical estimate of the fraction susceptible near the end of a major outbreak ((3.53) below), which is one of many expressions that we derive here.

We are not the first to attempt to approximate solutions of the SIR ODEs in the phase plane. In particular, van Herwaarden [27]—who was also motivated by (a different approach to) the stochastic extinction problem—presented some closely related approximations that are valid in specific regions of the phase plane. Here, we provide approximations that are uniformly valid throughout the phase plane, and we derive approximate expressions for a number of epidemiologically important quantities (e.g., the peak and minimum prevalence, and the minimum and maximum susceptible frequency, following initial disease invasion and following subsequent epidemics).

Our matching yields simple expressions that can, unlike previous results, be applied to an arbitrary number of epidemic cycles. Consequently, we obtain a complete analytical description of the phase plane trajectories (including the full transient dynamics), which allows us to find an accurate analytical approximation to the Poincaré map for the SIR model.

The related expressions that van Herwaarden [27] has presented previously—in addition to applying only to restricted subregions of the phase plane—depend on the numerical evaluation of integrals for which explicit analytical forms cannot be found. In contrast, our results are fully analytical closed-form expressions that are valid everywhere in phase space. We succeed by exploiting Lambert's W function [7] to invert implicit relations, and by asymptotic matching across branch cuts of the W function. The asymptotic techniques that we use are nontrivial and not part of the standard technical toolbox employed in mathematical epidemiology. Consequently, we present our analyses without assuming any familiarity with matched asymptotics, and we hope that in so doing we have made it easier for readers to apply the methods to other problems.

For convenience in using our approximations, all of our major results are summarized in Tables 2 and 3.

1.1. The SIR model with vital dynamics. Writing the proportions of the host population that are susceptible, infectious, and removed as X, Y, and Z, respectively, the standard SIR ODEs are [2]

$$\frac{\mathrm{d}X}{\mathrm{d}t} = \mu(1-X) - \beta XY\,, \tag{1.1a}$$

$$\frac{\mathrm{d}Y}{\mathrm{d}t} = (\beta X - \gamma - \mu)Y\,, \tag{1.1b}$$

$$\frac{\mathrm{d}Z}{\mathrm{d}t} = \gamma Y - \mu Z\,, \tag{1.1c}$$

where μ is the per capita rate of birth and death, β is the transmission rate, and γ is the recovery (or removal) rate. Our focus in this paper is on solutions of these deterministic equations (1.1), but elsewhere [25] we show how they can be used together with a branching process approximation to obtain accurate analytical results

[1] We find it convenient to pronounce "epsilon over Rnought" as "Eeyore" [21].

for the fully stochastic model (including the probability of pathogen extinction due to stochastic effects). In keeping with our stochastic analysis [25], we reserve S, I, and R for the *number* of individuals in each state. For the sake of clarity, we adopt the convention of using lowercase letters to indicate independent variables and uppercase to indicate dependent variables.

We henceforth work with dimensionless parameters. To that end, we first note that a natural timescale is the expected duration of an individual's infectious period,

$$T_{\text{inf}} = \frac{1}{\gamma + \mu}\,. \tag{1.2}$$

Expressing the *expected infectious period* in units of the expected host lifetime $(1/\mu)$, we define

$$\varepsilon = \frac{\mu}{\gamma + \mu}\,. \tag{1.3}$$

The *basic reproduction number* $(\mathcal{R}_0)$ is the product of the transmission rate β and the mean infectious period,

$$\mathcal{R}_0 = \frac{\beta}{\gamma + \mu}\,, \tag{1.4}$$

which gives the expected total number of new infections caused by a single infective individual introduced into a naïve population. We define a new time variable, $\tau = t/(\gamma + \mu)$, so that one time unit corresponds to the expected duration of an individual's infectious period. The SIR model then becomes

$$\frac{\mathrm{d}X}{\mathrm{d}\tau} = \varepsilon(1 - X) - \mathcal{R}_0 XY\,, \tag{1.5a}$$

$$\frac{\mathrm{d}Y}{\mathrm{d}\tau} = (\mathcal{R}_0 X - 1)Y\,. \tag{1.5b}$$

The sum $X(\tau) + Y(\tau) + Z(\tau) = 1$ for all $\tau \geq 0$, so the two equations above completely describe the dynamical system (1.1). Since $\mathcal{R}_0$ is the expected number of infections during the period ε, the expected time—in natural units—until the first infection is the ratio of ε and $\mathcal{R}_0$,

$$\epsilon = \frac{\varepsilon}{\mathcal{R}_0}\,; \tag{1.6}$$

ϵ turns out to be a better choice of small parameter to use in our analysis, because it leads to simpler asymptotic expressions.

Equations (1.5) have two nullclines. The y nullcline, $\frac{\mathrm{d}Y}{\mathrm{d}\tau} = 0$, is the line

$$x = \frac{1}{\mathcal{R}_0}\,, \tag{1.7a}$$

whereas the x nullcline, $\frac{\mathrm{d}X}{\mathrm{d}\tau} = 0$, is the curve

$$y = \epsilon\left(\frac{1}{x} - 1\right)\,. \tag{1.7b}$$

When $\mathcal{R}_0 > 1$, these two nullclines intersect at $(x_\star, y_\star)$, where

$$x_\star = \frac{1}{\mathcal{R}_0}\,, \tag{1.8a}$$

$$y_\star = \varepsilon\left(1 - \frac{1}{\mathcal{R}_0}\right) = \varepsilon(1 - x_\star)\,. \tag{1.8b}$$

It is well known that any trajectory departing from an initial point $(x_{\rm i}, y_{\rm i})$ in the positive cone $\{(x,y) : x > 0, y > 0\}$ eventually converges on a globally asymptomatically stable *endemic equilibrium* (EE) at $(x_\star, y_\star)$, whereas the *disease-free equilibrium* (DFE) at $(1,0)$ is a saddle attracting the set $\{(x,y) : y = 0\}$. Approach to the EE occurs via damped oscillations provided [10, eq. 13]

$$\varepsilon < \frac{4(\mathcal{R}_0 - 1)}{{\mathcal{R}_0}^2} = 4x_\star(1 - x_\star)\,. \tag{1.9}$$

This condition is satisfied for most diseases of interest; we restrict our focus to this typical behavior.

We will be primarily concerned with the phase-plane trajectories of (1.5), so rather than using those equations directly, we will make use of the phase-plane equations,

$$\frac{\mathrm{d}Y}{\mathrm{d}x} = \frac{(\mathcal{R}_0 x - 1)Y}{\varepsilon(1-x) - \mathcal{R}_0 xY} = \frac{(x - x_\star)Y}{\epsilon(1-x) - xY} \tag{1.10}$$

and

$$\frac{\mathrm{d}X}{\mathrm{d}y} = \frac{\varepsilon(1-X) - \mathcal{R}_0 Xy}{(\mathcal{R}_0 X - 1)y} = \frac{\epsilon(1-X) - Xy}{(X - x_\star)y}. \tag{1.11}$$

Thus, $Y(x)$ and $X(y)$ indicate phase-plane solutions where x (resp., y) is the independent variable, whereas we use $X(\tau)$ and $Y(\tau)$ to indicate the solution to the time-parametrized equations (1.5). We shall need both equations (1.10) and (1.11). Equation (1.10) (equation (1.11)) is singular where the susceptible (infectious) hosts attain their minimum and maximum density, $\underline{x}$ and $\overline{x}$ ($\underline{y}$ and $\overline{y}$), for a given cycle (these are points where nullclines, (1.7a) and (1.7b), are crossed). These singular points (see Figures 1 and 2) divide different branches of the multifunctions $Y(x)$ and $X(y)$, and we will need each equation to extend the solution beyond the singularities of the other. No exact analytical form is available for any of these turning points, but with our matched asymptotic expansions, we obtain asymptotic approximations to all of them (see Table 2 for a summary). We shall refer to the part of the trajectory above the x nullcline (1.7b) as the *epidemic phase* or simply as *epidemic* (e.g., we will speak of the *initial epidemic*, *second epidemic*, and so on) and the part below the x nullcline as the *trough*.

1.2. The method of matched asymptotic expansions. Given a small parameter ϵ, an *asymptotic sequence* is a collection of functions[2]

$$\{\varphi_j(\epsilon),\, j = 1, 2, \ldots\} \quad \text{such that} \quad \varphi_{j+1}(\epsilon) \ll \varphi_j(\epsilon) \tag{1.12}$$

(a typical choice is $\varphi_j(\epsilon) = \epsilon^{j-1}$, but as we shall see below, other choices are often necessary). Given an equation—which may be an ordinary or partial differential

[2]We use the Hardy–Vinogradov notation: $f(\epsilon) \ll g(\epsilon)$ if and only if $\lim_{\epsilon\to 0} \frac{f(\epsilon)}{g(\epsilon)} = 0$. We also use Landau's "O" notation where convenient: $f(\epsilon) = o(g(\epsilon))$ if $f(\epsilon) \ll g(\epsilon)$, and $f(\epsilon) = \mathcal{O}(g(\epsilon))$ if there exists a positive constant C such that $|f(\epsilon)| \le C|g(\epsilon)|$ as $\epsilon \to 0$.

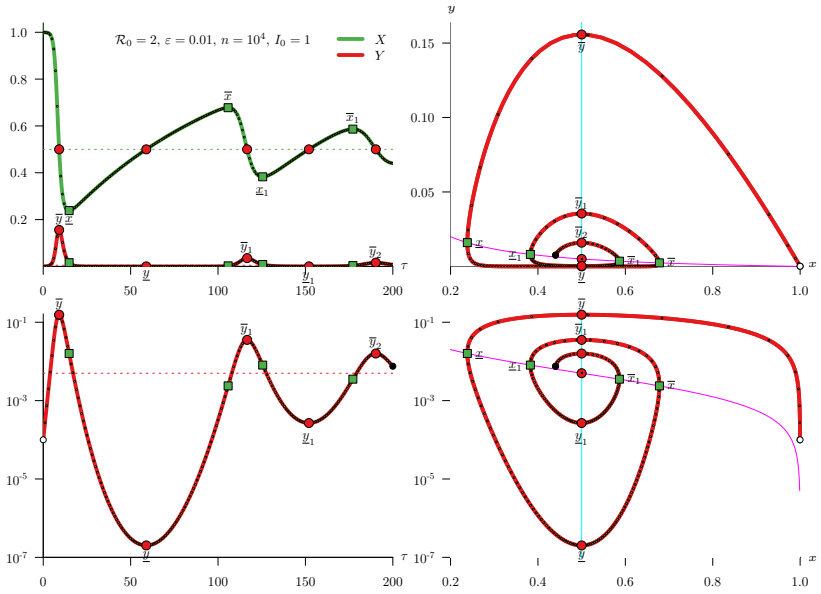

FIG. 1. *Sample solution of the SIR model* (1.1) *for* $\mathcal{R}_0 = 2$. *Top left: the frequencies of susceptible and infectious individuals. Symbols indicate the critical points of the curve of the corresponding color. The* j*th local minimum (maximum) of the susceptible (infective) frequency is labeled* $\underline{x}_j$ ($\overline{x}_j$) ($\underline{y}_j$ ($\overline{y}_j$)); *in* (3.46b), (3.47), *and* (3.48) *we give approximations to these optima. Dashed lines indicate the endemic equilibrium* (1.8) *of the model* (1.1). *Small yellow dots along trajectories are spaced by one time unit (the mean infectious period). Bottom left: the frequency of infectious individuals (on a log scale) as a function of time. Right: trajectories in the susceptible-infectious phase plane with the nullclines (top right: linear scale; bottom right: log scale). (Color online.)*

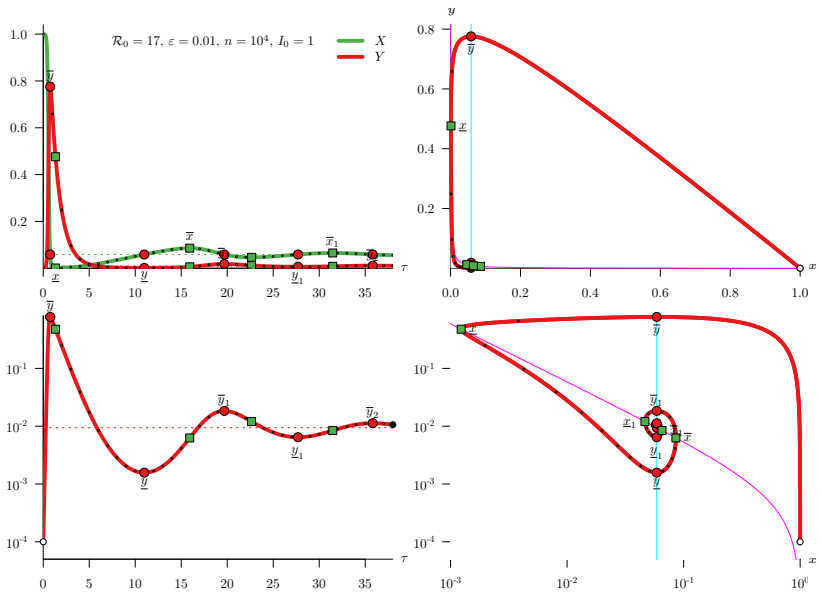

FIG. 2. *Sample solution of the SIR model* (1.1) *for* $\mathcal{R}_0 = 17$. *See caption to Figure* 1, *but note that unlike Figure* 1 *both axes are logarithmic in the bottom right panel here.*

equation—for an unknown function Y that depends on ϵ, we can look for a formal *asymptotic series* solution:

$$Y(x;\epsilon) = \sum_{j=0}^{\infty} Y_j(x)\varphi_j(\epsilon)\,. \tag{1.13}$$

Note that we do not demand that the series converge; the infinite upper limit on the sum is to indicate that one could in principle compute an arbitrary number of terms.

Substituting the formal series into the exact equation (1.10) and equating terms of common order $\varphi_j(\epsilon)$, we obtain a hierarchy of equations that can be solved sequentially for the $Y_j(x)$. The first few terms of such a series solution often yield a good approximation to the exact solution. However, this approach may fail in regions of rapid change (e.g., near boundaries or singularities) called *layers*,[3] especially in differential equations where one or more derivatives have coefficients depending on ϵ, which can make imposing all boundary (or initial or terminal) conditions impossible. The *method of matched asymptotic expansions* begins by identifying layers where different approximations better capture the correct behavior of the solution. These layers coincide with regions where some term in the equation is implicitly of size comparable to ϵ (i.e., of order $\eta(\epsilon)$ for some function η), even when it doesn't explicitly contain ϵ, so that neglecting terms including ϵ fails to capture the correct dynamics. *Boundary layers* refer to subsets of the domain adjacent to the boundary (where one of the dependent variables is small compared to some function of ϵ), whereas *interior layers* occur away from the boundaries (e.g., shear flow[4] in a vector field could result in a region where one or more derivatives is small compared to a function of ϵ). *Corner layers* arise where boundary and/or interior layers intersect. (For the SIR model that we study here, there are boundary and corner layers, but no interior layers.) The locations of these layers are fully determined *qualitatively* (e.g., "near the x-axis" or "where $\mathrm{d}X/\,\mathrm{d}\tau$ is small") but their quantitative width is characterized only up to an order of magnitude; one cannot exactly specify where the trajectory enters or departs a layer.

Outside of such layers, the so-called *outer solution* provides a good approximation to the exact solution, but inside the layers it fails to capture the correct qualitative behavior. Within a layer, rescaling of the independent and/or dependent variables by appropriately chosen factors $\eta(\epsilon)$ is used to amplify the local behavior, and the resulting equation is then solved via another asymptotic series to obtain an *inner solution* that performs well in the layer, but typically is a poor approximation outside the layer. Inner and outer solutions are bridged by determining values for the constants of integration in the inner and outer solutions so that the various solutions intersect, and can thus be combined into a continuous approximation to the solution. When a combined solution is continuous, but not differentiable, a *corner layer* (and *corner layer solution*) near the point of intersection can be included in the matching to form a smooth approximation to the true trajectory that performs equally well across the entire domain (a *uniform asymptotic solution*). We discuss the matching procedure in greater detail in section 3 below. Just as one cannot quantitatively specify the various layers, it is generally impossible to exactly characterize the domain of applicability of the corresponding solutions, hence the importance of matching to obtain a uniformly valid solution.

[3]The terminology reflects the origins of the method in fluid mechanics [1].

[4]Shearing flow refers to adjacent regions where a vector field has substantially different magnitudes.

TABLE 1

Estimates of parameters associated with the natural history of infection for a variety of diseases. The observed parameters are the basic reproduction number ($\mathcal{R}_0$), the mean latent period (T_{lat}), and the mean infectious period (T_{inf}). The values of the other parameters were derived using (1.2), (1.3), (1.6), and (1.8a). *Note that the mean intrinsic generation interval in the SIR model* (1.1) *is $T_{\text{gen}} = 1/\gamma \simeq T_{\text{inf}}$, whereas in the SEIR model (which includes an exposed state in which individuals are not yet infectious), $T_{\text{gen}} \simeq T_{\text{lat}} + T_{\text{inf}}$* [16, 6]*; consequently, SIR and SEIR dynamics correspond most closely if we set $1/\gamma$ in the SIR model to be the sum of the observed mean latent and infectious periods. We set $\mu = 0.02$/year to mimic human birth and death rates, and we compute $\varepsilon = \mu/(\gamma + \mu)$* (1.3). *Where original sources present a range, we have listed the midpoint. Many of the estimates come from Anderson and May* [2] *($\mathcal{R}_0$ from their Table* 4.1 [2, p. 70]*, and the mean latent and infectious periods from their Table* 3.1 [2, p. 31]*).*

Disease	$\mathcal{R}_0$	$x_\star$	T_{lat} (days)	T_{inf} (days)	$\varepsilon \times 10^3$	$\epsilon \times 10^3$	Source
measles	17	0.059	8	5	0.71	0.042	[2]
pertussis	17	0.059	8	14	1.2	0.071	[2]
mumps	12	0.08	15	6	1.1	0.092	[2]
chickenpox	11	0.091	10	5	0.82	0.075	[2]
COVID-19 (Delta)	6.8	0.15	5.8	14	1.1	0.16	[17]
rubella	6.5	0.15	10	7	0.93	0.14	[2]
scarlet fever	5.5	0.18	1.5	18	1	0.19	[2]
smallpox	4.5	0.22	15	7	1.2	0.27	[15]
COVID-19 (ancestral)	3	0.33	3.7	14	0.97	0.32	[17]
HIV	2.2	0.47	87	270	19	8.9	[12]
influenza (1918)	1.8	0.56	2	2.5	0.25	0.14	[20, 2]
Ebola	1.6	0.62	9.3	7	0.89	0.56	[29]
pneumonic plague	1.3	0.77	4.3	2.5	0.37	0.29	[9]

Table 1 lists estimates of natural history of infection parameters for a variety of common diseases. For the problem at hand, observing that infectious periods are typically of order days or weeks, whereas typical human lifetimes are longer than 50 years, we see that ϵ (1.6) will generally be quite small. Consequently, we anticipate that matched asymptotic solutions $Y(x;\epsilon)$ and $X(y;\epsilon)$ will provide good approximations to the exact solutions of (1.10) and (1.11). In subsequent sections, we derive and compare these asymptotic solutions to numerically computed trajectories for an illustrative parameter set (chosen with ε larger than for any acute infectious disease of humans so that discrepancies between the exact and asymptotic solutions are visible).

2. Outer and inner solutions. As a first step in our analysis, in this section we derive solutions in the various subdomains where different approximations are natural. We consider the subdomains in the order in which they are encountered along a trajectory. Then, in section 3, we match local approximations to obtain a single global approximation that is uniformly valid throughout phase space.

2.1. Outer solution. An outer solution is an asymptotic solution—obtained in the original variables—that captures the behavior of the exact solution in the majority of phase space. Replacing Y in (1.10) with

$$\overset{\text{out}}{Y}(x;\epsilon) = \sum_{j=0}^{\infty} \overset{\text{out}}{Y_j}(x)\epsilon^j\,, \tag{2.1}$$

and equating terms of similar order in ϵ, we obtain a hierarchy of equations that can be solved inductively for $\overset{\text{out}}{Y_0}(x), \overset{\text{out}}{Y_1}(x)$, and so on. The lowest order equation is

$$\frac{\mathrm{d}\overset{\text{out}}{Y_0}}{\mathrm{d}x} = \frac{x_\star}{x} - 1\,, \tag{2.2}$$

which has generic solution

$$\overset{\text{out}}{Y}_0(x) = \overset{\text{out}}{C}_0 - x + x_\star \ln x\,, \tag{2.3}$$

where $\overset{\text{out}}{C}_0$ is an arbitrary constant.[5] We can determine $\overset{\text{out}}{C}_0$ by specifying initial conditions $(x_{\text{i}}, y_{\text{i}})$, in which case (2.3) gives the phase-plane trajectory of the SIR ODEs without vital dynamics, i.e., for $\epsilon = 0$; see subsection 3.1.1 below. In subsection 3.1.2, we derive "effective initial conditions" that allow us to approximate subsequent epidemic waves.

2.2. *y*-axis boundary layer. For large values of $\mathcal{R}_0$, the trajectories of the SIR model approach the y-axis very closely, even when y is far from 0 (compare Figure 1 with $\mathcal{R}_0 = 2$ to Figure 2 with $\mathcal{R}_0 = 17$). Consequently, if $\mathcal{R}_0$ is large, then there will be substantial periods during which x will be $\mathcal{O}(\epsilon)$ or smaller, and we can no longer assume that the effects of terms proportional to ϵ in (1.10) can be safely neglected. Instead, we consider a boundary layer solution along the y-axis, making a change of variables $x = \epsilon\xi$ in (1.10) to get

$$\frac{\mathrm{d}Y}{\mathrm{d}\xi} = \frac{(\epsilon\xi - x_\star)Y}{1 - \epsilon\xi - \xi Y}\,. \tag{2.4}$$

Positing an asymptotic series solution,

$$\overset{\text{yb}}{Y}(\xi;\epsilon) = \sum_{j=0}^{\infty} \overset{\text{yb}}{Y}_j(\xi)\epsilon^j\,, \tag{2.5}$$

we get, to lowest order,

$$\frac{\mathrm{d}\overset{\text{yb}}{Y}_0}{\mathrm{d}\xi} = \frac{x_\star \overset{\text{yb}}{Y}_0}{\xi \overset{\text{yb}}{Y}_0 - 1}\,. \tag{2.6}$$

It is not immediately obvious how to solve this equation. However, if we invert the ODE, defining $\xi = \Xi_0(y)$, we have

$$\frac{\mathrm{d}\Xi_0}{\mathrm{d}y} = \frac{\Xi_0}{x_\star} - \frac{1}{x_\star y}\,, \tag{2.7}$$

and we can now find a solution using the method of integrating factors, which yields

$$\overset{\text{yb}}{X}_0(y) = \epsilon\,\Xi_0(y) = \frac{\epsilon}{x_\star}\, e^{\frac{y}{x_\star}} \left(E_1\left(\frac{y}{x_\star}\right) + \overset{\text{yb}}{C}_0 \right)\,, \tag{2.8}$$

where $E_1(z) = \int_z^\infty \frac{e^{-u}}{u}\,\mathrm{d}u$ is the exponential integral function (see, e.g., [23, section 6.2(i)]).

2.3. *x*-axis boundary layer. The outer solution $\overset{\text{out}}{Y}(x;\epsilon)$ (2.1) is a *function* of x and cannot have the same qualitative behavior as the exact trajectories, which have multiple branches as the fraction susceptible decreases to a minimum ($\underline{x}$) and then recovers (Figures 1 and 2). We thus seek a boundary layer solution $\overset{\text{xb}}{Y}(x;\epsilon)$ along the x-axis that will capture the dynamics when infectious hosts are rare (i.e., $y \ll 1$).

[5] Throughout, we adopt the convention that C, with any combination of sub- and/or superscripts, indicates a constant of integration.

Attempting to duplicate the analysis of subsection 2.2 above, we obtain the trivial solution $\overset{\text{xb}}{Y}(x;\epsilon) \equiv 0$ (see Appendix A). Since $0 < y \ll 1$ by assumption in this layer, we must conclude that an asymptotic series solution in powers of ϵ is not possible. Instead, it must be that $\overset{\text{xb}}{Y}(x;\epsilon)$ is *transcendentally small*, i.e., vanishes more rapidly than any power ϵ^j as $\epsilon \to 0$ [14, p. 4].

As a means to guess the asymptotic dependence of $\overset{\text{xb}}{Y}(x;\epsilon)$ on ϵ, we formally solve (1.10) from the point of entry to the boundary layer (x_{in}) to an arbitrary point within it (x) *assuming that* $Y(x;\epsilon)$ *is* $\mathcal{O}(\epsilon)$ *or smaller.* This yields

$$\overset{\text{xb}}{Y}(x;\epsilon) = \overset{\text{xb}}{Y}(x_{\text{in}};\epsilon) \exp\left(-\frac{1}{\epsilon} \int_{x_{\text{in}}}^{x} \frac{x_\star - u}{(1-u) - \frac{u}{\epsilon} Y(u;\epsilon)} \, \mathrm{d}u \right). \tag{2.9}$$

We first note that $x_{\text{in}} < x_\star$, so for $x_{\text{in}} < u < x_\star$, $1-u > x_\star - u > 0$ in the integrand above. Moreover, since $\overset{\text{xb}}{Y}(u;\epsilon)$ is transcendentally small we can expect that $\frac{u}{\epsilon}\overset{\text{xb}}{Y}(u;\epsilon) \ll 1-u$. Thus, the integrand can be expected to be positive for u in an interval wider than $(x_{\text{in}}, x_\star)$ and, consequently, the integral can be expected to be positive and $\mathcal{O}(1)$ with respect to ϵ. Finally, the coefficient $\overset{\text{xb}}{Y}(x_{\text{in}};\epsilon)$ is evaluated at the edge of the boundary layer and can therefore be expected to be $\mathcal{O}(1)$. Putting these heuristic insights together, we hypothesize that $\overset{\text{xb}}{Y}(x;\epsilon)$ is exponentially small in x with rate proportional to $\frac{1}{\epsilon}$. Consequently, we are led to what is known as a *WKB ansatz* [5, Chapter 10], that is, we postulate a solution of the form

$$\overset{\text{xb}}{Y}(x;\epsilon) = e^{-\frac{1}{\epsilon}\phi(x;\epsilon)} \tag{2.10}$$

for some nonnegative function $\phi(x;\epsilon)$ that can be expanded in an asymptotic series in powers of ϵ. Substituting this ansatz (2.10) into (1.10) gives us

$$\frac{1}{\epsilon}\frac{\mathrm{d}\phi}{\mathrm{d}x} = \frac{x_\star - x}{\epsilon(1-x) - x e^{-\frac{1}{\epsilon}\phi(x;\epsilon)}}, \tag{2.11}$$

for which we posit a series solution,

$$\phi(x;\epsilon) = \sum_{j=0}^{\infty} \phi_j(x)\epsilon^j, \tag{2.12}$$

so that

(2.13)

$$\begin{aligned}
&e^{-\frac{1}{\epsilon}\phi(x;\epsilon)} \\
&\quad = e^{-\frac{1}{\epsilon}\phi_0(x)} e^{-\phi_1(x)} e^{-\epsilon\phi_2(x) - \epsilon^2\phi_3(x) + \cdots} \\
&\quad = e^{-\frac{1}{\epsilon}\phi_0(x)} e^{-\phi_1(x)} \left(1 - \left(\epsilon\phi_2(x) + \epsilon^2\phi_3(x) + \cdots\right) + \frac{1}{2!}\left(\epsilon\phi_2(x) + \epsilon^2\phi_3(x) + \cdots\right)^2 + \cdots \right) \\
&\quad = e^{-\frac{1}{\epsilon}\phi_0(x)} e^{-\phi_1(x)} \left(1 - \epsilon\phi_2(x) + \epsilon^2 \left(\frac{\phi_2(x)^2}{2} - \phi_3(x) \right) + \cdots \right),
\end{aligned}$$

which is transcendentally small on any set where $\phi_0(x)$ is strictly positive (below we determine conditions under which $\phi_0(x) > 0$ on at least part of the interval $(0,1)$). If $\phi_0(x) > 0$, then the term $e^{-\frac{1}{\epsilon}\phi(x;\epsilon)}$ is transcendentally small and we can omit it in (2.11) to obtain

$$\frac{\mathrm{d}\phi_0}{\mathrm{d}x} = \frac{x_\star - x}{1-x}\,, \tag{2.14a}$$

$$\frac{\mathrm{d}\phi_j}{\mathrm{d}x} = 0\,, \qquad j = 1, 2, \ldots \tag{2.14b}$$

and hence

$$\phi_0(x) = C_0^\phi - x - (1 - x_\star)\ln(1-x)\,, \tag{2.15}$$

$$\phi_j(x) = C_j^\phi\,, \qquad j = 1, 2, \ldots \tag{2.16}$$

From the derivative (2.14a), we see that $\phi_0(x)$ is increasing for $x < x_\star$, is decreasing for $x > x_\star$, and has a vertical asymptote for $x = 1$. In particular, provided

$$C_0^\phi < x_\star + (1 - x_\star)\ln(1 - x_\star)\,, \tag{2.17}$$

$\phi_0(x)$ will be strictly positive on some subinterval of $(0, 1)$, as required. Inserting (2.15) and (2.16) in (2.13), we have an approximate solution in the x-axis boundary layer,

$$\overset{\mathrm{xb}}{Y}(x;\epsilon) = (1-x)^{-\frac{1}{\epsilon}(1-x_\star)}\, e^{\frac{1}{\epsilon}(C_0^\phi - x) + C_1^\phi}\,. \tag{2.18}$$

2.4. Corner layers. Close to the minimum susceptible frequency ($\underline{x}$), our outer (2.3) and inner (2.18) solutions have tangents of positive and negative slope, respectively (see Figure 4), and thus meet in a nondifferentiable corner, which we address by seeking a corner layer solution [14, p. 67]. The trajectories have vertical slope at $\underline{x}$, i.e., $\frac{\mathrm{d}Y}{\mathrm{d}x}$ is singular, so we will instead work with $\frac{\mathrm{d}X}{\mathrm{d}y}$. The increase from $\underline{x}$ is caused by importation of new susceptible hosts at a rate proportional to ϵ [see (1.11)], so we would expect the "turn-around" (change in sign of derivative) only when the frequency of infectives is sufficiently low that the first term dominates the second term in the numerator of (1.11), i.e., when y is $\mathcal{O}(\epsilon)$. We therefore amplify the behavior near the x-axis, making a change of variable, $y = \epsilon\upsilon$, which converts (1.11) to

$$\frac{\mathrm{d}X}{\mathrm{d}\upsilon} = \epsilon\frac{1 - X - X\upsilon}{(X - x_\star)\upsilon}. \tag{2.19}$$

Positing a series solution

$$\overset{\mathrm{cor}}{X}(\upsilon;\epsilon) = \sum_{j=0}^{\infty} \overset{\mathrm{cor}}{X}_j(\upsilon)\epsilon^j \tag{2.20}$$

yields, to lowest order, $\frac{\mathrm{d}\overset{\mathrm{cor}}{X}_0}{\mathrm{d}\upsilon} = 0$, so $\overset{\mathrm{cor}}{X}_0$ is constant,

$$\overset{\mathrm{cor}}{X}_0(\upsilon) = \overset{\mathrm{cor}}{C}_0\,. \tag{2.21}$$

The next order term is

$$\frac{\mathrm{d}\overset{\mathrm{cor}}{X}_1}{\mathrm{d}\upsilon} = -\left(\frac{1 - \overset{\mathrm{cor}}{C}_0}{x_\star - \overset{\mathrm{cor}}{C}_0}\right)\frac{1}{\upsilon} + \left(\frac{\overset{\mathrm{cor}}{C}_0}{x_\star - \overset{\mathrm{cor}}{C}_0}\right), \tag{2.22}$$

with solution

$$\overset{\mathrm{cor}}{X}_1(\upsilon) = -\left(\frac{1 - \overset{\mathrm{cor}}{C}_0}{x_\star - \overset{\mathrm{cor}}{C}_0}\right)\ln\upsilon + \left(\frac{\overset{\mathrm{cor}}{C}_0}{x_\star - \overset{\mathrm{cor}}{C}_0}\right)\upsilon + \overset{\mathrm{cor}}{C}_1\,. \tag{2.23}$$

We now insert (2.21) and (2.23) in (2.20), and convert back to the original variable y. Noting that $\ln \upsilon = \ln y + \ln \epsilon^{-1}$, we obtain

(2.24)
$$\overset{\text{cor}}{X}(y;\epsilon) = \overset{\text{cor}}{C}_0 + \left(\frac{\overset{\text{cor}}{C}_0}{x_\star - \overset{\text{cor}}{C}_0}\right) y - \epsilon \ln \epsilon^{-1} \left(\frac{1-\overset{\text{cor}}{C}_0}{x_\star - \overset{\text{cor}}{C}_0}\right) - \epsilon \left[\left(\frac{1-\overset{\text{cor}}{C}_0}{x_\star - \overset{\text{cor}}{C}_0}\right) \ln y - \overset{\text{cor}}{C}_1\right] + \mathcal{O}(\epsilon^2).$$

This solution contains a term of order $\epsilon \ln \epsilon^{-1}$, which is intermediate between $\mathcal{O}(1)$ and $\mathcal{O}(\epsilon)$, and which we did not include in our proposed asymptotic series in υ (2.20). The emergence of such a term when switching back to original variables is known as "transcendental switchback" [24, p. 71]. When this phenomenon occurs it is necessary to go back and include the intermediate order explicitly in the asymptotic sequence at the outset, as it may lead to novel terms that are essential for matching. Thus, we replace our initial ansatz (2.20) with

$$\overset{\text{cor}}{X}(\upsilon;\epsilon) = \overset{\text{cor}}{X}_0(\upsilon) + \epsilon \ln \epsilon^{-1} \overset{\text{cor}}{X}_{\ln}(\upsilon) + \epsilon \overset{\text{cor}}{X}_1(\upsilon) + \mathcal{O}(\epsilon^2), \tag{2.25}$$

which includes a term of order $\epsilon \ln \epsilon^{-1}$ in addition to powers of ϵ. Inserting (2.25) in (2.19) we obtain a new hierarchy of ODEs, with one new equation,

$$\frac{\mathrm{d}\overset{\text{cor}}{X}_{\ln}}{\mathrm{d}y} = 0, \tag{2.26}$$

which yields a new constant,

$$\overset{\text{cor}}{X}_{\ln}(y) \equiv \overset{\text{cor}}{C}_{\ln}. \tag{2.27}$$

Our revised expansion is

$$\overset{\text{cor}}{X}(y;\epsilon) = \overset{\text{cor}}{C}_0 + \left(\frac{\overset{\text{cor}}{C}_0}{x_\star - \overset{\text{cor}}{C}_0}\right) y + \epsilon \ln \epsilon^{-1} \left[\overset{\text{cor}}{C}_{\ln} - \left(\frac{1-\overset{\text{cor}}{C}_0}{x_\star - \overset{\text{cor}}{C}_0}\right)\right] - \epsilon \left[\left(\frac{1-\overset{\text{cor}}{C}_0}{x_\star - \overset{\text{cor}}{C}_0}\right) \ln y - \overset{\text{cor}}{C}_1\right] + \mathcal{O}(\epsilon^2), \tag{2.28}$$

which differs from (2.28) only in that it includes $\overset{\text{cor}}{C}_{\ln}$ in the $\mathcal{O}(\epsilon \ln \epsilon^{-1})$ term. Below, in subsection 3.1.2, we will see that the additional degree of freedom provided by the constant $\overset{\text{cor}}{C}_{\ln}$ is essential to successfully match other asymptotic solutions.

Remark 1. While this section concerns dynamics near $\underline{x}$, a virtually identical analysis provides a corner solution near $\overline{x}$, where the fraction susceptible is at its maximum prior to a second epidemic wave. In particular, we again have a solution of the form (2.28), albeit for different values of the constants $\overset{\text{cor}}{C}_0$ and $\overset{\text{cor}}{C}_1$. We will refer to the corner solutions near $\underline{x}$ and $\overline{x}$ as the "left" and "right" corner solutions, $\overset{\text{lc}}{X}$ and $\overset{\text{rc}}{X}$, respectively.

2.5. Scaled exponential and Lambert *W* functions. To match our various solutions, some functions of x, some functions of y, we need to write all expressions as functions of the same variable. For our matching, the common variable will be y, which is facilitated by two functions that we introduce in this section.

The expression ze^z occurs frequently in our analysis, with z often being a nontrivial expression itself. Consequently, in order to reduce equation clutter and emphasize patterns in expressions more clearly, we define the *scaled exponential function*,

$$\mathscr{E}(z) = z\,e^z\,. \tag{2.29}$$

The second function is the *Lambert W function* [7], a transcendental multifunction defined by the implicit relation

$$\mathscr{E}(W(z)) = z\,. \tag{2.30}$$

Thus, W is a Lambert W function if $\mathscr{E}$ is its left inverse. There are countably many such functions of a complex argument, leading to countably many branches $W_i(z)$. There are two branches that are real-valued for real arguments. We will need both real-valued branches, which are denoted W_{-1} and W_0. They have overlapping domains, but nonoverlapping ranges,

$$W_{-1} : \big[-\frac{1}{e}, 0\big) \to (-\infty, -1]\,, \tag{2.31a}$$

$$W_0 : \big[-\frac{1}{e}, \infty\big) \to [-1, \infty)\,. \tag{2.31b}$$

Thus, these two branches meet at $(\mathscr{E}(-1), -1)$,

$$W_{-1}(\mathscr{E}(-1)) = W_0(\mathscr{E}(-1)) = -1\,. \tag{2.32}$$

For any i, $\mathscr{E}$ is also a *partial* right inverse of W_i, i.e., $W_i(\mathscr{E}(z)) = z$ on *part* of the domain of $\mathscr{E}$. The set on which $W_i(\mathscr{E}(z)) = z$ depends on i; for $i \in \{-1, 0\}$,

$$\begin{aligned} W_{-1}(\mathscr{E}(z)) &= z \quad \text{if } z \le -1\,, \\ W_0(\mathscr{E}(z)) &= z \quad \text{if } z \ge -1\,. \end{aligned} \tag{2.33}$$

However, $W_i(\mathscr{E}(z))$ is well-defined outside the region on which $\mathscr{E}$ is a right inverse, and it is on the domain where $W_i(\mathscr{E}(z)) \neq z$ that we frequently need to evaluate it. Indeed, the explicit final size formula for the SIR model (and many other models) is [18, eq. (A.2)]

$$Z(\mathcal{R}_0) = 1 + \frac{1}{\mathcal{R}_0} W_0(\mathscr{E}(-\mathcal{R}_0))\,. \tag{2.34}$$

Graphs of $\mathscr{E}(z)$ and $W_i(\mathscr{E}(z))$ are shown in Figure 3.

We briefly recall some series and asymptotic expansions of the Lambert W function that we will need below. See [7] for details and proofs.

(i) Implicitly differentiating the identity $\mathscr{E}(W_i(z)) = W_i(z)e^{W_i(z)} = z$ and solving for $\frac{\mathrm{d}W_i}{\mathrm{d}z}$ one finds that

$$\frac{\mathrm{d}W_i}{\mathrm{d}z} = \frac{W_i}{z(1+W_i)}\,. \tag{2.35}$$

(ii) Applying the Lagrange inversion theorem (see, e.g., [8, p. 180]) to the power series for $\mathscr{E}(z)$, one finds that near 0,

$$W_0(z) = \sum_{n=1}^{\infty} \frac{(-n)^{n-1}}{n!} z^n = z + \mathcal{O}(z^2)\,, \tag{2.36}$$

with radius of convergence $\frac{1}{e}$.

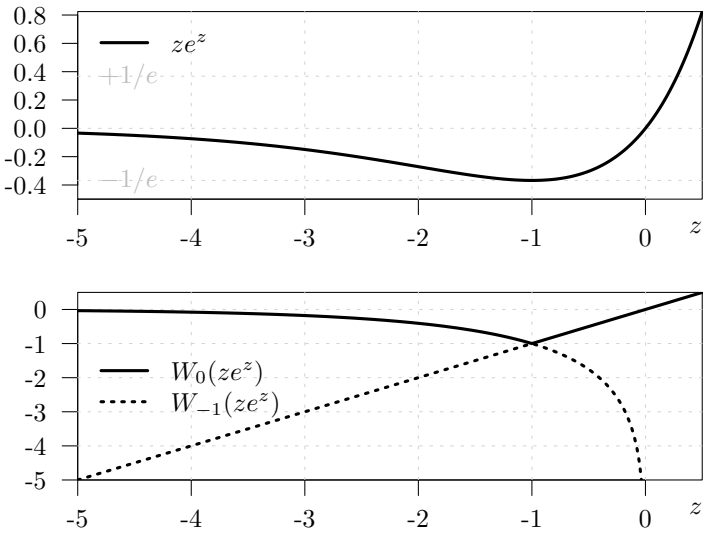

FIG. 3. $\mathscr{E}(z) = ze^z$ (2.29) *and Lambert W functions* (2.30) *evaluated at* $\mathscr{E}(z)$.

(iii) For large z, there is a (convergent) asymptotic series representation,

$$W_0(z) = L_1 - L_2 + \sum_{m=0}^{\infty}\sum_{n=1}^{\infty} \frac{(-1)^m}{m!} \frac{L_2^n}{L_1^{m+n}}, \qquad z \to \infty, \tag{2.37}$$

where $L_1 = \ln z$ and $L_2 = \ln(\ln z)$. The same expansion applies for $W_{-1}(z)$ as $z \to 0^-$ if one replaces L_1 and L_2 with $\tilde{L}_1 = \ln(-z)$ and $\tilde{L}_2 = \ln(-\ln(-z))$.

(iv) We will also find it useful to expand

$$f_i(z) = W_i(-Ae^{-A-B+z}) = W_i(\mathscr{E}(-A)e^{-B}e^z) \tag{2.38}$$

in a series about $z = 0$ for various values of A and B. Using (2.35), we find

$$f_i(z) = W_i(\mathscr{E}(-A)e^{-B}) + \frac{W_i(\mathscr{E}(-A)e^{-B})}{1 + W_i(\mathscr{E}(-A)e^{-B})} z + \mathcal{O}(z^2). \tag{2.39}$$

In particular, (2.33) tells us that if $B = 0$ then

$$f_i(z) = -A - \frac{A}{1-A} z + \mathcal{O}(z^2) \qquad \text{if} \quad i = 0 \text{ and } A \le 1 \quad \text{or} \quad i = -1 \text{ and } A \ge 1. \tag{2.40}$$

2.6. Inverting the outer and inner solutions. To facilitate matching, we now exploit the scaled exponential $\mathscr{E}$ (2.29) and Lambert's W (2.30) to invert some of our asymptotic solutions.

Our outer solution (2.3) can be rearranged by setting $\overset{\text{out}}{Y}_0(x) = y$ and using (2.29),

$$-\frac{1}{x_\star} e^{(y - \overset{\text{out}}{C}_0)/x_\star} = \mathscr{E}\Big(-\frac{x}{x_\star}\Big). \tag{2.41}$$

Next, using (2.33), we have

$$W_i\Big(-\frac{1}{x_\star} e^{(y-\overset{\text{out}}{C}_0)/x_\star}\Big) = W_i\left(\mathscr{E}\Big(-\frac{x}{x_\star}\Big)\right) = -\frac{x}{x_\star}, \tag{2.42}$$

where the $i=-1$ branch is to be used in the *right half-plane* $\{(x,y): x \geq x_\star\}$ (since $W_{-1} \leq -1$, (2.31a)), whereas the $i=0$ branch is to be used in the *left half-plane* $\{(x,y): x \leq x_\star\}$ (since $W_0 \geq -1$, (2.31b)). From (2.42), we obtain

$$\overset{\text{out}}{X}{}_0^i(y) = x = -x_\star W_i\left(-\frac{1}{x_\star} e^{(y-\overset{\text{out}}{C}{}_0)/x_\star}\right). \tag{2.43}$$

Thus, the inversion yields a multifunction $\overset{\text{out}}{X}{}_0^i(y)$ with two branches, both of which we need. These branches correspond to the growth ($i=-1$) and decline ($i=0$) phases of the epidemic, which meet at $y=\overset{\text{out}}{Y}{}_0(x_\star)$ (the maximum of $\overset{\text{out}}{Y}{}_0(x)$, and thus also the upper bound of the domain of its inverse, $\overset{\text{out}}{X}{}_0^i(y)$).

Similarly, we can invert our inner solution in the x-axis boundary layer (2.18) to get

$$\overset{\text{xb}}{X}{}_0^i(y) = 1 + (1-x_\star) W_i\left(-\frac{1}{1-x_\star} e^{-\frac{1-C_0^\phi}{1-x_\star}} \left(\frac{e^{C_1^\phi}}{y}\right)^{\frac{\epsilon}{1-x_\star}}\right), \tag{2.44}$$

where now the $i=-1$ and $i=0$ branches give the solution for $x \leq x_\star$ and $x \geq x_\star$, respectively (the opposite of the situation for $\overset{\text{out}}{X}{}_0^i(y)$ in (2.43), where $i=-1$ and $i=0$ correspond to the right and left half-planes, respectively).

Remark 2. Once the constants have been determined by matching, we will be able to exploit the resulting symmetry (and the function $\mathscr{E}$) to simplify the inverted expressions considerably.

3. Matched asymptotic solutions. We now turn to the task of identifying the unknown constants in the solutions above and combining these local approximations into a uniform approximation of the trajectory. Suppose we have two or more solutions defined at different asymptotic scales (e.g., our outer (subsection 2.1) and corner (subsection 2.4) solutions). The local solutions are obtained by imposing a scale on dependent or independent variables (e.g., we supposed x is $\mathcal{O}(1)$ to get the outer solution and assumed y was $\mathcal{O}(\epsilon)$ to get the corner solution, whereas we obtained the y-axis boundary layer solution (subsection 2.2) by assuming X is $\mathcal{O}(\epsilon)$). In practice, however, each local solution remains valid over some larger domain that can be characterized with another asymptotic scale. Matching (see, e.g., [14, section 2.1]) is achieved by considering an intermediate scale $\eta=\eta(\epsilon)$ on which all solutions remain valid. Solutions to be matched are evaluated at $x=\eta x_\eta$ (or $y=\eta y_\eta$) for some x_η (or y_η) independent of ϵ (for readability, we suppress the explicit dependence of η itself on ϵ). The constants of integration (e.g., $\overset{\text{cor}}{C}{}_0$, C_1^ϕ, etc.) are then chosen so that the two solutions agree as well as possible (i.e., so that they coincide on as many orders as possible when both are expanded as an asymptotic series). The *matched solution* is obtained by summing the component solutions—with the choice of constants of integration that maximizes their mutual agreement—and subtracting their common *overlap* (the sum of all terms occurring in both asymptotic series).

To illustrate the process without getting bogged down in details, suppose $F(x)$ and $G(x)$ are outer and inner (e.g., boundary layer) asymptotic series approximations for a given (exact) function $E(x)$. Moreover, suppose we have

$$F(x) = f_0(x) + f_1(x)\varphi_1(\epsilon) + f_2(x)\varphi_2(\epsilon) + f_3(x)\varphi_3(\epsilon) + \mathcal{O}(\varphi_4(\epsilon)), \tag{3.1}$$

$$G(x) = g_2(x)\varphi_2(\epsilon) + g_3(x)\varphi_3(\epsilon) + \mathcal{O}(\varphi_4(\epsilon)), \tag{3.2}$$

where the functions f_j and g_j contain arbitrary constants, and $\{\varphi_j\}$ is an asymptotic sequence (subsection 1.2), which typically refines the asymptotic sequences initially

defined for the outer and inner solutions. If, say, the constants in $f_2(x)$ and $g_2(x)$ can be chosen so that these functions coincide exactly for all x, then $f_2(x)\varphi_2(\epsilon) = g_2(x)\varphi_2(\epsilon)$ is the overlap, and our matched approximation to $E(x)$ would be

$$F(x) + G(x) - f_2(x)\varphi_2(\epsilon)\,. \tag{3.3}$$

If it were possible to choose the values of constants so that F and G agree in more than one order, so the overlap contains multiple orders (the more the better), then the resulting matched solution would be smoother (just as matching both a function and its derivative at a single point leads to a smoother approximation at that point).

The matched solution has the virtue of being a valid approximation in both the inner and outer domains, so that one does not need to decide a priori which local solution (e.g., outer, boundary, or corner) best approximates a given part of the trajectory.

In what follows, we will give a detailed treatment of the first matching (which includes the outer, corner, and x-axis boundary layer solutions) and describe the second matching (which also includes the y-axis boundary layer solution) much more briefly. For easy reference, we summarize our results in Tables 2 and 3 and list the matching constants in Table 4. We compare the first and second matchings to the numerically evaluated trajectory in Figures 4(a) and 4(b), respectively. We find excellent agreement for all inital conditions $(x_{\mathrm{i}}, y_{\mathrm{i}})$ from which the trajectory does not approach the y-axis too closely; more precisely, our approximations are accurate unless $x_{\mathrm{f}}(x_{\mathrm{i}}, y_{\mathrm{i}}) \ll \epsilon$, where $x_{\mathrm{f}}(x_{\mathrm{i}}, y_{\mathrm{i}})$ is given in (3.8) below.

TABLE 2

Approximations of quantities of epidemiological interest for the trajectory of (1.5) *that emanates from* $(x_{\mathrm{i}}, y_{\mathrm{i}})$. *Each entry may depend upon entries above it in the table (but never on entries below). These quantities are used in our approximations to the full trajectories in Table* 3. *We use "(KM)" to indicate quantities that are exact for the Kermack–McKendrick SIR model* without *vital dynamics* ($\epsilon = 0$). *With vital dynamics* ($\epsilon > 0$), *the peak prevalence* $\overline{y}_0$ *is an approximation, and there is no "final" size, but the quantity* x_{f} *appears in the approximation to the minimum fraction susceptible* ($\underline{x}_0$). *Replacing* x_{i} *by* $x_{\mathrm{i},j}$ *as defined in* (3.46) *gives asymptotic approximations for the* j*th epidemic wave. We discuss the effective initial condition* ($x_{\mathrm{i},2}$) *in subsection* 3.1.3. *The expressions for the minimum and maximum susceptible densities* ($\underline{x}_0, \overline{x}_0$) *are identical except that* $\underline{x}_0$ *is evaluated at* x_{f} *and* $\overline{x}_0$ *is evaluated at* $x_{\mathrm{i},2}$. *In these expressions, note that* $(x_{\mathrm{f}}, \epsilon(\frac{1}{x_{\mathrm{f}}} - 1))$ *and* $(x_{\mathrm{i},2}, \epsilon(\frac{1}{x_{\mathrm{i},2}} - 1))$ *are points on the* x *nullcline* $\mathrm{d}X/\mathrm{d}\tau = 0$. *We write the formulae for* $\underline{x}_0$ *and* $\overline{x}_0$ *as compactly as possible here; see* (3.29) *for the same expression written out with separate terms for each asymptotic order.*

Quantity		**Expression**	**Equation**
Equilibrium susceptible density	$x_\star$	$\frac{1}{\mathcal{R}_0}$	(1.8a)
Peak prevalence (KM)	$\overline{y}_0$	$y_{\mathrm{i}} + x_{\mathrm{i}} - x_\star(1 + \ln(x_{\mathrm{i}}/x_\star))$	(3.7)
Final size (KM)	x_{f}	$-x_\star W_0(\mathscr{E}(-x_{\mathrm{i}}/x_\star)e^{-y_{\mathrm{i}}/x_\star})$	(3.8)
Minimum prevalence	$\underline{y}_0$	$\overline{y}_0(\frac{1-x_{\mathrm{f}}}{1-x_\star})^{\frac{1-x_\star}{\epsilon}} e^{-\frac{x_\star - x_{\mathrm{f}}}{\epsilon}} e^{-\mathrm{Ein}(\overline{y}_0/x_\star)}$	(3.30)
Minimum susceptible density	$\underline{x}_0$	$x_{\mathrm{f}} + \epsilon\frac{1-x_{\mathrm{f}}}{x_\star - x_{\mathrm{f}}}(1 + \ln(\epsilon(\frac{1}{x_{\mathrm{f}}} - 1)/\overline{y}_0))$	(3.29)
Effective initial condition	$x_{\mathrm{i},2}$	$1 + (1 - x_\star)W_0(\mathscr{E}(-\frac{1-x_{\mathrm{f}}}{1-x_\star}))$	(3.33)
Maximum susceptible density	$\overline{x}_0$	$x_{\mathrm{i},2} - \epsilon\frac{1-x_{\mathrm{i},2}}{x_{\mathrm{i},2} - x_\star}(1 + \ln(\epsilon(\frac{1}{x_{\mathrm{i},2}} - 1)/\overline{y}_0))$	(3.43)
Peak prevalence, second wave	$\overline{y}_{0,2}$	$x_{\mathrm{i},2} - x_\star(1 + \ln(x_{\mathrm{i},2}/x_\star))$	(3.45)

TABLE 3

Matched solutions for SIR trajectories. The quantities $x_\star$, $x_{\rm f}$, $\overline{y}_0$, $x_{{\rm i},2}$, and $\overline{y}_{0,2}$ are expressed in terms of the parameters $\mathcal{R}_0$ and ϵ in Table 2. Left and right corner solutions are valid in a neighborhood of the points $(x_{\rm f},0)$ and $(x_{{\rm i},2},0)$, respectively (and are identical up to swapping $x_{\rm f}$ and $x_{{\rm i},2}$). Left and right matched solutions are uniformly valid to the left and right of the y nullcline $(x=x_\star)$. Setting $(x_{\rm i},y_{\rm i})=(1,0)$ gives a first epidemic wave emanating from the DFE. Asymptotic approximations for the jth epidemic wave (for $j\geq 1$) are obtained by replacing $x_{\rm i}$ with $x_{{\rm i},j}$, $x_{\rm f}$ by $x_{{\rm f},j}$, $x_{{\rm i},2}$ by $x_{{\rm i},j+1}$, $\overline{y}_0$ by $\overline{y}_{0,j}$, and $\overline{y}_{0,2}$ and $\overline{y}_{0,j+1}$ in the expressions and domains (see (3.46)*). For each of the outer, inner, and left and right corner solutions, the equation reference first is the "raw" expression with undetermined matching constants (the matched values are listed in Table* 4*) and then the "matched" expression with the matched values of the constants inserted. Gray text is used to emphasize a factor in the x-axis boundary layer approximation and a term in the left matched solution that appear when we include the y-axis boundary layer approximation in the matching; Figure* 4(a) *shows results without the gray quantities, whereas Figure* 4(b) *shows the improvement obtained by including them.*

Solution	Notation	Expression	Branch (i)	Domain	Equation
Outer	$\overset{\rm out}{X}{}^i_0(y,x_{\rm i},y_{\rm i})$	$-x_\star W_i(\mathscr{E}(-x_{\rm i}/x_\star)e^{(y-y_{\rm i})/x_\star})$	$\begin{cases}0 & x\leq x_\star\\ -1 & x\geq x_\star\end{cases}$	$[0,\overline{y}_0]$	(2.43), (3.6)
y-axis bdry	$\overset{\rm yb}{X}_0(y)$	$\frac{\epsilon}{x_\star}e^{-\frac{y}{x_\star}}\left(E_1(\frac{y}{x_\star})-E_1(\frac{\overline{y}_0}{x_\star})\right)$	–	$[\underline{y}_0,\overline{y}_0]$	(3.52)
Left corner	$\overset{\rm lc}{X}(y;\epsilon)$	$x_{\rm f}+\frac{x_{\rm f}}{x_\star-x_{\rm f}}y+\epsilon\frac{1-x_{\rm f}}{x_\star-x_{\rm f}}\ln(\overline{y}_0/y)$	–	$[\underline{y}_0,\overline{y}_0]$	(2.28), (3.28)
x-axis bdry	$\overset{\rm xb}{X}{}^i_0(y)$	$1+(1-x_\star)\times$ $W_i\Big(\mathscr{E}(-\frac{1-x_{\rm f}}{1-x_\star})(\frac{\overline{y}_0}{y})^{\frac{\epsilon}{1-x_\star}}$ $e^{-\frac{\epsilon}{1-x_\star}\,\mathrm{Ein}(\overline{y}_0/x_\star)}\Big)$	$\begin{cases}-1 & x\leq x_\star\\ 0 & x\geq x_\star\end{cases}$	$[\underline{y}_0,\overline{y}_0]$	(3.59)
Right corner	$\overset{\rm rc}{X}(y;\epsilon)$	$x_{{\rm i},2}-\frac{x_{{\rm i},2}}{x_{{\rm i},2}-x_\star}y-\epsilon\frac{1-x_{{\rm i},2}}{x_{{\rm i},2}-x_\star}\ln(\overline{y}_0/y)$	–	$[\underline{y}_0,\overline{y}_{0,2}]$	(2.28), (3.36)
Matched, left	$\overleftarrow{X}(y;\epsilon)$	$\overset{\rm out}{X}{}^0_0(y,x_{\rm i},y_{\rm i})+\overset{\rm xb}{X}{}^{-1}_0(y)-x_{\rm f}$ $+\overset{\rm yb}{X}_0(y)+\frac{\epsilon}{x_\star}\Big(\ln(\frac{y}{\overline{y}_0})+\mathrm{Ein}(\frac{\overline{y}_0}{x_\star})\Big)$	–	$[\underline{y}_0,\overline{y}_0]$	(3.61)
Matched, right	$\overrightarrow{X}(y;\epsilon)$	$\overset{\rm out}{X}{}^{-1}_0(y,x_{{\rm i},2},0)+\overset{\rm xb}{X}{}^0_0(y;\epsilon)-x_{{\rm i},2}$	–	$[\underline{y}_0,\overline{y}_{0,2}]$	(3.42)

3.1. Matching outer, corner, and x-axis boundary layer solutions.

3.1.1. Kermack and McKendrick's phase plane solution. Given an initial condition $(x_{\rm i},y_{\rm i})$, the constant of integration in (2.3) is readily found to be

$$\overset{\rm out}{C}{}_0 = y_{\rm i}+x_{\rm i}-x_\star\ln x_{\rm i}\,, \tag{3.4}$$

$$\text{so that}\quad \overset{\rm out}{Y}{}_0(x,x_{\rm i},y_{\rm i}) = y_{\rm i}+x_{\rm i}-x+x_\star\ln\left(\frac{x}{x_{\rm i}}\right), \tag{3.5}$$

which is the phase plane solution first discovered by KM for the SIR model *without* vital dynamics. Equivalently, using (2.43), we can express the solution as a function of y,

$$\begin{aligned}\overset{\rm out}{X}{}^i_0(y,x_{\rm i},y_{\rm i}) &= -x_\star\,W_i\big(-(x_{\rm i}/x_\star)\,e^{(y-y_{\rm i}-x_{\rm i})/x_\star}\big)\\ &= -x_\star\,W_i\big(\mathscr{E}(-x_{\rm i}/x_\star)\,e^{(y-y_{\rm i})/x_\star}\big)\,.\end{aligned} \tag{3.6}$$

Provided $x_{\rm i}\geq x_\star$ and $y_{\rm i}\geq 0$, the solution (3.5) is nonnegative and concave, with two positive roots ($x_{\rm f}\in(0,x_\star)$ and another in $(x_\star,1)$), and a unique maximum $\overline{y}_0$ at $x_\star$,

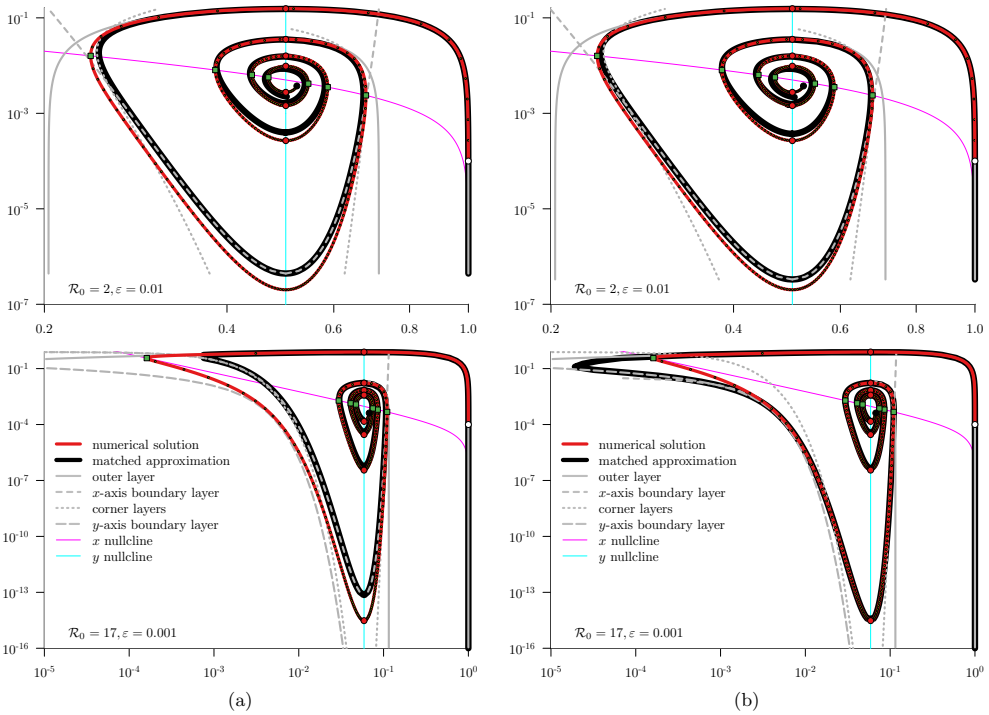

FIG. 4. *Solutions of the SIR ODEs* (1.1) *and approximations (Table* 3*). Top panels:* $\mathcal{R}_0 = 2$ *and* $\varepsilon = 0.01$*. Bottom panels:* $\mathcal{R}_0 = 17$ *and* $\varepsilon = 0.001$*, similar to measles and whooping cough (Table* 1*). Various outer and inner approximations are shown in gray, and the matched approximation is in black. The numerically computed solutions are red, as in Figures* 1 *and* 2*. The right panels include the y-axis boundary layer approximation* $(\overset{yb}{Y})$ *in the matching. All trajectories are plotted on a log-log scale in order to emphasize discrepancies between the red and black curves.*

$$\overline{y}_0(x_i, y_i) = \overset{\text{out}}{Y}_0(x_\star, x_i, y_i) = y_i + x_i - x_\star\left(1 + \ln(x_i/x_\star)\right). \tag{3.7}$$

Note that $\overline{y}_0(x_i, y_i)$ and $x_f(x_i, y_i)$ are the true peak prevalence and final size for the SIR model without vital dynamics ($\epsilon = 0$) started from (x_i, y_i); $\overline{y}_0$ only approximates the peak prevalence for the model with vital dynamics, and there is no "final" size if there is a continuous source of new susceptibles. Nevertheless, we informally refer to x_f as the "final size" for convenience (note that there *is* a minimum fraction susceptible, $\underline{x}$, near $x_f(x_i, y_i)$; see (3.29) below).

Using the $i = 0$ branch to give the solution in the half-plane $x \le x_\star$, (3.6) gives us an explicit expression for $x_f(x_i, y_i)$ [18],

$$x_f(x_i, y_i) = \overset{\text{out}}{X}_0^0(0) = -x_\star W_0\left(\mathscr{E}(-x_i/x_\star)e^{-y_i/x_\star}\right). \tag{3.8}$$

The series expansion for Lambert's W function (2.36) then yields

$$\begin{aligned} x_f(x_i, y_i) &= x_i e^{-(x_i+y_i)/x_\star} + \mathcal{O}\big((x_i/x_\star)e^{-2(x_i+y_i)/x_\star}\big) \\ &= x_i e^{-\mathcal{R}_0(x_i+y_i)} + \mathcal{O}\big(\mathcal{R}_0(x_i e^{-\mathcal{R}_0(x_i+y_i)})^2\big), \end{aligned} \tag{3.9}$$

so the final size is exponentially small in $\mathcal{R}_0$, with a correction of exponentially smaller order.

When there is no risk of ambiguity, we suppress the dependence on $x_{\rm i}$ and $y_{\rm i}$ and write $\overset{\rm out}{Y}_0(x)$, $\overset{\rm out}{X}{}^i_0(x)$, $\overline{y}_0$, and $x_{\rm f}$. Note that $[x_{\rm f}, x_{\rm i}]$ is the interval on which $\overset{\rm out}{Y}_0(x)$ is nonnegative, and thus its domain for practical purposes; its range, $[0, \overline{y}_0]$, is the domain for its inverse $\overset{\rm out}{X}{}^i_0(y)$.

3.1.2. Matching in the left half-plane ($x \le x_\star$). Our next step is to match the outer solution $\overset{\rm out}{X}{}^0_0(y)$ ((3.6) with initial point $(x_{\rm i}, y_{\rm i})$) with the corner solution $\overset{\rm cor}{X}(y;\epsilon)$ (2.28). Note that although we assume the initial point lies in the *right* half-plane (i.e., $x_\star \le x_{\rm i}$), in the present subsection it is the $i = 0$ branch of the outer solution that we need because we are investigating only the part of the trajectory that lies in the *left* half-plane.

In order to consider the behavior near $(x_{\rm f}, 0)$ on scales intermediate between the outer solution (3.6) and the corner solution (2.28), we take $y = \eta y_\eta$ with

$$\epsilon \ll \eta \ll 1 \tag{3.10}$$

(we haven't yet identified an appropriate intermediate scale, but examples that satisfy (3.10) include $\eta = \epsilon^{1/2}$ and $\eta = \epsilon \ln \epsilon^{-1}$).

Inserting $(x_{\rm i}, y_{\rm i})$ in the outer solution (3.6), expanding it using (2.39), and using (3.8) to find $x_{\rm f}$, we obtain

$$\overset{\rm out}{X}{}^0_0(\eta y_\eta) = -x_\star\, W_0\Big(\mathscr{E}(-x_{\rm i}/x_\star)\, e^{-y_{\rm i}}\, e^{\eta y_\eta / x_\star}\Big) = x_{\rm f} + \eta \frac{x_{\rm f}}{x_\star - x_{\rm f}} y_\eta + \mathcal{O}(\eta^2)\,. \tag{3.11}$$

On the other hand, inserting $y = \eta y_\eta$ in the corner solution (2.28) and expanding

$$\ln(\eta y_\eta) = -\ln \eta^{-1} + \ln y_\eta\,, \tag{3.12}$$

we can write

$$\begin{aligned} \overset{\rm cor}{X}(\eta y_\eta;\epsilon) = \overset{\rm cor}{C}_0 &+ \eta \frac{\overset{\rm cor}{C}_0}{x_\star - \overset{\rm cor}{C}_0} y_\eta + \epsilon \ln \epsilon^{-1} \left(\overset{\rm cor}{C}_{\ln} - \frac{1 - \overset{\rm cor}{C}_0}{x_\star - \overset{\rm cor}{C}_0} \right) \\ &+ \epsilon \ln \eta^{-1} \left(\frac{1 - \overset{\rm cor}{C}_0}{x_\star - \overset{\rm cor}{C}_0} \right) - \epsilon \left(\frac{1 - \overset{\rm cor}{C}_0}{x_\star - \overset{\rm cor}{C}_0} \ln(y_\eta) - \overset{\rm cor}{C}_1 \right) + \mathcal{O}(\epsilon^2). \end{aligned} \tag{3.13}$$

If we now refine our initial assumption (3.10) to $\epsilon \ln \epsilon^{-1} \ll \eta \ll (\epsilon \ln \epsilon^{-1})^{1/2} \ll 1$, then in the expansions (3.11), (3.13) each term has a distinct asymptotic order, ensuring that

$$\epsilon \ll \epsilon \ln \eta^{-1} \ll \epsilon \ln \epsilon^{-1} \ll \eta \ll (\epsilon \ln \epsilon^{-1})^{1/2} \ll 1\,. \tag{3.14}$$

Consequently, if we take

$$\overset{\rm cor}{C}_0 = x_{\rm f} \qquad \text{and} \qquad \overset{\rm cor}{C}_{\ln} = \frac{1 - \overset{\rm cor}{C}_0}{x_\star - \overset{\rm cor}{C}_0} = \frac{1 - x_{\rm f}}{x_\star - x_{\rm f}}, \tag{3.15}$$

then the two solutions (3.11), (3.13) coincide to[6] $\mathcal{O}(\epsilon \ln \epsilon^{-1})$. For the moment, $\overset{\rm cor}{C}_1$ remains undetermined, but we will use it to match with the inner solution.

[6]The assumptions $\epsilon \ll \eta$ and $\eta \ll (\epsilon \ln \epsilon^{-1})^{1/2}$ (3.14) together imply that $\epsilon^2 \ll \eta^2 \ll \epsilon \ln \epsilon^{-1}$, which is necessary to ensure that the $\mathcal{O}(\eta^2)$ terms in (3.11) are negligible in comparison to $\epsilon \ln \epsilon^{-1}$.

To match the corner layer solution with the inner (x-axis boundary layer) solution we now let η denote a different asymptotic order,

$$e^{-\frac{C}{\epsilon}} \ll \eta \ll \epsilon \ll 1 \qquad \text{for all} \quad C > 0. \tag{3.16}$$

Since we are interested in $x \le x_\star$, as noted after (2.44) we must use the $i = -1$ branch of the inner solution $\overset{\text{xb}}{X}{}_0^i(y)$. We will use (2.39) to derive an asymptotic expansion for $\overset{\text{xb}}{X}{}_0^{-1}(y)$, which motivates us—after some algebraic exploration—to set

$$C_0^\phi = c_0^\phi - (1 - x_\star)\ln(1 - c_0^\phi)\,. \tag{3.17}$$

This choice for C_0^ϕ in (2.44) leads to

$$\begin{aligned}\overset{\text{xb}}{X}{}_0^{-1}(\eta y_\eta) &= 1 + (1 - x_\star)\,W_{-1}\left(-\frac{1 - c_0^\phi}{1 - x_\star} e^{-\frac{1 - c_0^\phi}{1 - x_\star}} \left(\frac{e^{C_1^\phi}}{\eta y_\eta}\right)^{\frac{\epsilon}{1 - x_\star}}\right) \\ &= 1 + (1 - x_\star)\,W_{-1}\left(\mathscr{E}\left(-\frac{1 - c_0^\phi}{1 - x_\star}\right) e^{\epsilon\psi(\eta y_\eta)}\right),\end{aligned} \tag{3.18a}$$

$$\text{where} \qquad \psi(y) = \frac{1}{1 - x_\star}\ln\left(\frac{e^{C_1^\phi}}{y}\right). \tag{3.18b}$$

Our assumption that $\eta \ll \epsilon \ll 1$ (3.16) implies that $\eta \ll \epsilon \ll \epsilon\ln\epsilon^{-1} \ll \epsilon\ln\eta^{-1} \ll 1$. Observing that $\epsilon\,\psi(\eta y_\eta) = \mathcal{O}(\epsilon\ln\eta^{-1})$, we can therefore apply (2.38) and (2.40) to (3.18) to obtain

$$\overset{\text{xb}}{X}{}_0^{-1}(\eta y_\eta) = c_0^\phi + \epsilon\left(\frac{1 - c_0^\phi}{x_\star - c_0^\phi}\right)\left(C_1^\phi - \ln y_\eta\right) + \epsilon\ln\eta^{-1}\left(\frac{1 - c_0^\phi}{x_\star - c_0^\phi}\right) + \mathcal{O}(\epsilon^2). \tag{3.19}$$

Furthermore, comparing (3.13) and (3.19) to order $\mathcal{O}(\epsilon)$, we see that the overlap is maximized by taking

$$c_0^\phi = \overset{\text{cor}}{C}{}_0 = x_{\text{f}} \quad \text{(see (3.15))}, \quad \text{and} \quad \overset{\text{cor}}{C}{}_1 = \frac{1 - x_{\text{f}}}{x_\star - x_{\text{f}}} C_1^\phi\,, \tag{3.20}$$

whereas C_1^ϕ is yet to be determined.

With the values of the constants determined above, the outer (3.11) and corner (3.13) solutions have a common overlap of

$$x_{\text{f}} + \eta\frac{x_{\text{f}}}{x_\star - x_{\text{f}}} y_\eta\,, \tag{3.21}$$

whereas for the corner and inner (3.19) solutions, the overlap is

$$x_{\text{f}} - \epsilon\frac{1 - x_{\text{f}}}{x_\star - x_{\text{f}}} x_{\text{f}}(C_1^\phi - \ln y_\eta) + \epsilon\ln\eta^{-1}\frac{1 - x_{\text{f}}}{x_\star - x_{\text{f}}}. \tag{3.22}$$

Summing the outer (3.11), inner (3.19), and corner (3.13) solutions and subtracting these two overlaps yields a matched solution to the left of $x_\star$,

$$\overleftarrow{X}(y;\epsilon) = \overset{\text{out}}{X}{}_0^0(y;\epsilon) + \overset{\text{xb}}{X}{}_0^{-1}(y;\epsilon) - x_{\text{f}}\,. \tag{3.23}$$

(Subtracting the overlaps (3.21), (3.22) removes the corner solution (3.13) from the matched solution; the corner was nonetheless necessary to determine the matching

constant c_0^{ϕ}.) For the matched solution to be continuous, $\overleftarrow{X}$ must agree at $(x_\star, \overline{y}_0)$ with the outer solution (3.6) in the right half-plane, i.e., we need

$$\overleftarrow{X}(\overline{y}_0;\epsilon) = x_\star = \overset{\text{out}}{X}{}_0^{-1}(\overline{y}_0)\,. \tag{3.24}$$

This requirement is satisfied provided

$$C_1^{\phi} = \ln \overline{y}_0. \tag{3.25}$$

While we have used the $i=-1$ branch to find C_0^{ϕ} and C_1^{ϕ}, these same constants appear in the identical expression for the $i=0$ branch (2.44), hence yielding the solution for $x \geq x_\star$ without further work. Thus, substituting the values of the matching constants C_0^{ϕ} and C_1^{ϕ} into (2.44), we find that the x-axis boundary layer inner solution expressed as a function of y is

$$\overset{\text{xb}}{X}{}_0^{i}(y;\epsilon) = 1 + (1-x_\star)\, W_i\!\left(\mathscr{E}\Big(-\frac{1-x_{\text{f}}}{1-x_\star}\Big)\left(\frac{\overline{y}_0}{y}\right)^{\frac{\epsilon}{1-x_\star}}\right). \tag{3.26}$$

Substituting the values of C_0^{ϕ} and C_1^{ϕ} into (2.18) gives us an alternative description of the boundary layer dynamics as a function of x,

$$\overset{\text{xb}}{Y}(x;\epsilon) = \overline{y}_0 \left(\frac{1-x_{\text{f}}}{1-x}\right)^{\frac{1-x_\star}{\epsilon}} e^{-\frac{x-x_{\text{f}}}{\epsilon}}. \tag{3.27}$$

Inserting the values of $\overset{\text{cor}}{C}_0$ and $\overset{\text{cor}}{C}_{\ln}$ (3.15), and $\overset{\text{cor}}{C}_1$ [(3.20), (3.25)], into (2.28), we see that the corner solution near x_{f} is

$$\overset{\text{lc}}{X}(y;\epsilon) = x_{\text{f}} + \frac{x_{\text{f}}}{x_\star - x_{\text{f}}} y + \epsilon \frac{x_{\text{f}}}{x_\star - x_{\text{f}}} \ln\left(\frac{\overline{y}_0}{y}\right), \tag{3.28}$$

where, as noted in Remark 1, we use "lc" to emphasize that this is a "left corner" solution lying in the left half-plane. We will consider a right corner solution below.

Minimum susceptible proportion. The left corner solution (3.28) approximately characterizes the trajectory near $\underline{x}$, the point where the fraction susceptible is minimized. Solving $\mathrm{d}\overset{\text{cor}}{X}/\mathrm{d}\upsilon = 0$ (2.19), we find that its minimum occurs at $\upsilon = \left(\frac{1}{x_{\text{f}}} - 1\right)$, whence the minimum fraction susceptible is approximately

$$\begin{aligned} \underline{x}_0 = \underline{x}_0(x_{\text{f}}) = \overset{\text{lc}}{X}\left(\epsilon\left(\frac{1}{x_{\text{f}}}-1\right);\epsilon\right) &= x_{\text{f}} + \epsilon\left(\frac{1-x_{\text{f}}}{x_\star - x_{\text{f}}}\right)\left[1 + \ln\left(\frac{\epsilon\left(\frac{1}{x_{\text{f}}}-1\right)}{\overline{y}_0}\right)\right] \\ &= x_{\text{f}} - \epsilon \ln \epsilon^{-1}\left(\frac{1-x_{\text{f}}}{x_\star - x_{\text{f}}}\right) + \epsilon\left(\frac{1-x_{\text{f}}}{x_\star - x_{\text{f}}}\right)\left[1 + \ln\left(\frac{\frac{1}{x_{\text{f}}}-1}{\overline{y}_0}\right)\right]. \end{aligned} \tag{3.29}$$

Prevalence trough. Substituting $x = x_\star$ into (3.27) gives us an approximation to $\underline{y}$, the minimum fraction infectious after the initial epidemic,

$$\underline{y}_0 = \overline{y}_0 \left(\frac{1-x_{\text{f}}}{1-x_\star}\right)^{\frac{1-x_\star}{\epsilon}} e^{-\frac{x_\star - x_{\text{f}}}{\epsilon}}. \tag{3.30}$$

Point of entry into the boundary layer. With the known values of the matching constants c_0^{ϕ} (3.20) and C_0^{ϕ} (3.17), we can write the leading term (2.15) in the asymptotic series (2.13), by which we obtained the inner solution, as

$$\phi_0(x) = (x - x_{\mathrm{f}}) - (1 - x_\star) \ln\left(\frac{1 - x_{\mathrm{f}}}{1 - x}\right). \tag{3.31}$$

The inner solution ((2.10), (2.18)) is proportional to $e^{-\frac{\phi_0(x)}{\epsilon}}$ (see (2.13)). Consequently, as we observed in subsection 2.3, the inner solution is trancendentally small in ϵ^{-1} on the set of x where $\phi_0(x) > 0$, whereas we see from (3.31) that $\phi_0(x_{\mathrm{f}}) = 0$. Thus, $(x_{\mathrm{f}}, Y(x_{\mathrm{f}}))$ is effectively the point of entry into the boundary layer: $e^{-\phi_0(x_{\mathrm{f}})/\epsilon} = 1 = \mathcal{O}(1)$, whereas for $x > x_{\mathrm{f}}$ (near x_{f}), $e^{-\phi_0(x)/\epsilon}$ is transcendentally small.

Point of exit from the boundary layer. In addition to x_{f}, $\phi_0(x)$ has a second root that we denote $x_{\mathrm{i},2}$ (for reasons that will become clear when we complete the matching). The point $x_{\mathrm{i},2}$ is where the trajectory exits the boundary layer: $\phi_0(x) > 0$ for $x \in (x_{\mathrm{f}}, x_{\mathrm{i},2})$, and $\phi_0(x) < 0$ for $x > x_{\mathrm{i},2}$. Just as we used a corner solution at x_{f} to characterize the transition from the outer solution to the inner solution entering the boundary layer,[7] a right corner solution at $x_{\mathrm{i},2}$ allows us to match the inner solution to a new outer solution corresponding to the second epidemic wave. To find an expression for $x_{\mathrm{i},2}$ we substitute $x = x_{\mathrm{i},2}$ into (3.31) and obtain

$$(1 - x_\star) \ln\left(\frac{1 - x_{\mathrm{f}}}{1 - x_{\mathrm{i},2}}\right) - (x_{\mathrm{i},2} - x_{\mathrm{f}}) = 0. \tag{3.32}$$

As in subsection 2.6, we solve this for $x_{\mathrm{i},2}$ using the Lambert W-function and find

$$x_{\mathrm{i},2} = 1 + (1 - x_\star)\, W_0\left(\mathscr{E}\left(-\frac{1 - x_{\mathrm{f}}}{1 - x_\star}\right)\right). \tag{3.33}$$

3.1.3. Matching in the right half-plane ($x \geq x_\star$). As in subsection 3.1.2, our matched inner layer solution (3.26) can be continued to the right of $x_\star$ by switching from the $i = -1$ to the $i = 0$ branch of Lambert's W. As we observed above, this boundary layer solution is transcendentally small for $x < x_{\mathrm{i},2}$, i.e., for all y such that $\overset{x\mathrm{b}}{X}{}_0^0(y;\epsilon) < x_{\mathrm{i},2}$. As the trajectory leaves the boundary layer, the fraction infectious goes from transcendentally small to $\mathcal{O}(1)$, until eventually the rate of infection exceeds the rate of replenishment of susceptible hosts by host vital dynamics, causing a second *turn-around*, where now the fraction susceptible starts to decrease. Our inner solution fails to capture this turn-around, which we now address, as in subsection 3.1.2, with a (right) corner solution near $x_{\mathrm{i},2}$.

We begin by considering our solutions on a scale η that is intermediate between $\mathcal{O}(\epsilon)$ and transcendentally small (3.16). Expanding the inner solution $\overset{x\mathrm{b}}{X}{}_0^0(\eta y_\eta)$ as in (3.19), we find that

$$\overset{x\mathrm{b}}{X}{}_0^0(\eta y_\eta) = x_{\mathrm{i},2} + \epsilon \frac{1 - x_{\mathrm{i},2}}{x_\star - x_{\mathrm{i},2}} \left(\ln \overline{y}_0 - \ln y_\eta\right) + \epsilon \ln \eta^{-1} \frac{1 - x_{\mathrm{i},2}}{x_\star - x_{\mathrm{i},2}} + \mathcal{O}(\epsilon^2). \tag{3.34}$$

[7] The pedantic reader (or author) might observe that the corner solution was obtained by assuming that $y = \mathcal{O}(\epsilon)$, whereas the outer and inner solutions correspond to $y = \mathcal{O}(1)$ and transcendentally small y, respectively. This apparent incongruity is reconciled by considering the solutions in a very small neighborhood of x_{f}: for $C > 0$, $\exp(-\frac{\phi_0(x_{\mathrm{f}} + C\epsilon \ln \epsilon^{-1})}{\epsilon}) = \mathcal{O}(\epsilon)$, and it is in this $\mathcal{O}(\epsilon \ln \epsilon^{-1})$ neighborhood of x_{f} that the solutions match, which is reflected in the scaling (3.14) required when matching the solutions in subsection 3.1.2.

Comparing this expansion to the corner series (3.13), we see that a maximal matching is obtained by taking

$$\overset{\text{cor}}{C}_0 = x_{\text{i},2}\,, \qquad \overset{\text{cor}}{C}_{\ln} = \frac{1-x_{\text{i},2}}{x_\star - x_{\text{i},2}}\,, \qquad \text{and} \quad \overset{\text{cor}}{C}_1 = \frac{1-x_{\text{i},2}}{x_\star - x_{\text{i},2}} \ln \overline{y}_0\,. \tag{3.35}$$

Substituting these values in (3.13) gives us the right corner solution,

$$\overset{\text{rc}}{X}(y;\epsilon) = x_{\text{i},2} + \frac{x_{\text{i},2}}{x_\star - x_{\text{i},2}} y + \epsilon \frac{1-x_{\text{i},2}}{x_\star - x_{\text{i},2}} \ln\left(\frac{\overline{y}_0}{y}\right) + \mathcal{O}(\epsilon^2)\,. \tag{3.36}$$

Beyond the turn-around at the corner, we are again in the domain of validity of the outer solution $\overset{\text{out}}{X}{}^i_0(y)$ (2.43), where we now use the $i=-1$ branch as we are matching in the right half-plane. To match corner and outer solutions, we choose $\epsilon \ll \eta \ll 1$ and set $y = \eta y_\eta$. As we did for C_0^ϕ in the inner solution in subsection 3.1.2, equation (3.17), we make a change of constants,

$$\overset{\text{out}}{C}_0 = \overset{\text{out}}{c}_0 - x_\star \ln \overset{\text{out}}{c}_0\,, \tag{3.37}$$

in (2.43) to get

$$\overset{\text{out}}{X}{}^{-1}_0(\eta y_\eta) = -x_\star W_{-1}\Big(-(\overset{\text{out}}{c}_0/x_\star) e^{-\frac{\overset{\text{out}}{c}_0 - \eta y_\eta}{x_\star}}\Big) = -x_\star W_{-1}\Big(\mathscr{E}\big(-(\overset{\text{out}}{c}_0/x_\star)\big) e^{\frac{\eta y_\eta}{x_\star}}\Big)\,. \tag{3.38}$$

Expanding this expression using (2.38) and (2.40) then gives us

$$\overset{\text{out}}{X}{}^{-1}_0(\eta y_\eta) = \overset{\text{out}}{c}_0 + \eta \frac{\overset{\text{out}}{c}_0}{x_\star - \overset{\text{out}}{c}_0} y_\eta + \mathcal{O}(\eta^2)\,. \tag{3.39}$$

Substituting $y = \eta y_\eta$ in (3.36) and expanding exactly as in (3.13), we find that (3.36) and (3.39) agree to order $\mathcal{O}(\eta)$ provided

$$\overset{\text{out}}{c}_0 = x_{\text{i},2}\,. \tag{3.40}$$

Thus, the matched solution is

$$\overset{\text{out}}{X}{}^{-1}_0(y, x_{\text{i},2}, 0) = -x_\star W_{-1}\left(\mathscr{E}\left(-x_{\text{i},2}/x_\star\right) e^{y/x_\star}\right)\,. \tag{3.41}$$

As in our derivation of the left solution $\overleftarrow{X}(y;\epsilon)$ (3.23), we sum the outer (3.41), inner (3.26), and corner (3.36) solutions and subtract their overlaps to obtain a uniform asymptotic solution to the right of $x_\star$,

$$\overrightarrow{X}(y;\epsilon) = \overset{\text{out}}{X}{}^{-1}_0(y, x_{\text{i},2}) + \overset{x\text{b}}{X}{}^0_0(y;\epsilon) - x_{\text{i},2}\,. \tag{3.42}$$

Smoothly joined approximations. We now have consistent approximations to the trajectory that starts from $(x_{\text{i}}, y_{\text{i}})$. From the initial time until the peak prevalence is reached, the trajectory is in the right half-plane and we use the KM solution (3.5) for the model without vital dynamics ($\epsilon = 0$). We then continue into the left half-plane using $\overleftarrow{X}(y;\epsilon)$ (3.23) until the first prevalence trough is reached at $x = x_\star$, where we switch to $\overrightarrow{X}(y;\epsilon)$ (3.42) to approximate the rising segment of the second epidemic. The switches from one approximation to another are differentiable and always occur when $x = x_\star$, and the combined approximation is uniformly valid (i.e., valid to the

same order throughout the phase plane). We compare $\overleftarrow{X}(y;\epsilon)$ (3.23) and $\overrightarrow{X}(y;\epsilon)$ (3.42) to numerically evaluated trajectories in Figure 4(a).

Effective initial conditions. Comparing $\overset{\text{out}}{X}{}_0^{-1}(y, x_{\text{i},2}, 0)$ (3.41) to $\overset{\text{out}}{X}{}_0^{i}(y, x_{\text{i}}, y_{\text{i}})$ (3.6), we see that $(x_{\text{i},2}, 0)$ is an *effective initial condition* for the second epidemic: if $(x_{\text{i},2}, 0)$ were used as the initial state in the KM ($\epsilon = 0$) solution, the resulting trajectory would meet the second rise of the actual solution as it curves up from the left in the phase plane at (approximately) $\overline{x}_0$ (see below). Thus, while $(x_{\text{i},2}, 0)$ is not a point on the actual trajectory, it represents an "effective" initial condition that would give rise to the true dynamics after the end (i.e., trough) of the first epidemic. This observation motivates our choice of notation $x_{\text{i},2}$.

Maximum fraction susceptible. Just as the minimum value of the left corner solution near x_{f} (3.28) gives an estimate of $\underline{x}$ (3.29), the maximum value for the right corner solution near $x_{\text{i},2}$ (3.36) gives us an estimate of $\overline{x}$, the maximum fraction susceptible before a second epidemic wave,

$$\overline{x}_0 = \overline{x}_0(x_{\text{i},2}) = x_{\text{i},2} - \epsilon \frac{1 - x_{\text{i},2}}{x_{\text{i},2} - x_\star} \left(1 + \ln\left(\epsilon\left(\frac{1}{x_{\text{i},2}} - 1\right) \Big/ \overline{y}_0\right)\right), \tag{3.43}$$

which occurs at $y = \epsilon\left(\frac{1}{x_{\text{i},2}} - 1\right)$.

Peak prevalence for the second wave. Writing (3.41) as a function of x via KM's formula (3.5),

$$\overset{\text{out}}{Y}{}_0(x) = x_{\text{i},2} - x + x_\star \ln(x/x_{\text{i},2}), \tag{3.44}$$

we can also obtain an approximation of the second epidemic's prevalence peak,

$$\overline{y}_{0,2} \approx x_{\text{i},2} - x_\star(1 + \ln(x_{\text{i},2}/x_\star)). \tag{3.45}$$

3.1.4. Matching beyond the first epidemic wave. Our uniform matched asymptotic solutions, $\overleftarrow{X}$ (3.23) and $\overrightarrow{X}$ (3.42), were derived for the first epidemic wave starting from $(x_{\text{i}}, y_{\text{i}})$. However, a straightforward observation allows us to use the formulae for $\overleftarrow{X}$ and $\overrightarrow{X}$ for the entire trajectory (i.e., all epidemic waves). Other than $x_\star$ and ϵ (or the more fundamental parameters $\mathcal{R}_0$ and ε), the only parameters on which our approximations depend are the initial condition $(x_{\text{i}}, y_{\text{i}})$, the approximate maximum size of the epidemic $(\overline{y}_0)$ (equation (3.7)), the final size of the epidemic without vital dynamics (x_{f}) (equation (3.8)), and the effective initial condition for the next epidemic $(x_{\text{i},2})$ (equation (3.33)).

Epidemic iteration. We write $x_{\text{i},j}$ for the effective initial condition associated with the jth epidemic wave. Setting $x_{\text{i},1} = x_{\text{i}}$, $y_{\text{i},1} = y_{\text{i}}$, and $y_{\text{i},j} = 0$ for $j > 1$, we iteratively obtain $x_{\text{i},j+1}$ from $x_{\text{i},j}$ and $y_{\text{i},j}$ by computing

$$x_{\text{f},j} = x_{\text{f}}(x_{\text{i},j}, y_{\text{i},j}) = -x_\star W_0\big(\mathscr{E}(-x_{\text{i},j}/x_\star) e^{y_{\text{i},j}/x_\star}\big), \tag{3.46a}$$

$$\overline{y}_{0,j} = \overline{y}_0(x_{\text{i},j}, y_{\text{i},j}) = y_{\text{i},j} + x_{\text{i},j} - x_\star\left(1 + \ln(x_{\text{i},j}/x_\star)\right), \tag{3.46b}$$

$$x_{\text{i},j+1} = 1 + (1 - x_\star) W_0\left(\mathscr{E}\left(-\frac{1 - x_{\text{f},j}}{1 - x_\star}\right)\right). \tag{3.46c}$$

The intermediate quantities, $x_{\text{f},j}$ and $\overline{y}_{0,j}$, are the final fraction susceptible and maximal fraction infectious, respectively, for the SIR model *without* vital dynamics ($\varepsilon = 0$) with initial condition $(x_{\text{i},j}, y_{\text{i},j})$.

Substituting these expressions (3.46) into $\overleftarrow{X}$ (3.23) and $\overrightarrow{X}$ (3.42) provides uniform matched asymptotic approximations to the full jth epidemic wave for all $j \geq 1$: $\overleftarrow{X}$ maps to $[\underline{x}_{0,j}, x_\star]$ and $\overrightarrow{X}$ maps to $[x_\star, \overline{x}_{0,j}]$, where

$$\underline{x}_{0,j} = \underline{x}_0(x_{\mathrm{f},j}, \overline{y}_{0,j}) = x_{\mathrm{f},j} + \epsilon \frac{1 - x_{\mathrm{f},j}}{x_\star - x_{\mathrm{f},j}} \left(1 + \ln\left(\epsilon \left(\frac{1}{x_{\mathrm{f},j}} - 1\right) / \overline{y}_{0,j}\right)\right), \tag{3.47a}$$

$$\overline{x}_{0,j} = \overline{x}_0(x_{\mathrm{i},j+1}, \overline{y}_{0,j}) = x_{\mathrm{i},j+1} - \epsilon \frac{1 - x_{\mathrm{i},j+1}}{x_{\mathrm{i},j+1} - x_\star} \left(1 + \ln\left(\epsilon \left(\frac{1}{x_{\mathrm{i},j+1}} - 1\right) / \overline{y}_{0,j}\right)\right). \tag{3.47b}$$

Poincaré map. If we think of the y nullcline ($x = x_\star$) as a surface of section, we can use (3.46) to explicitly write down the associated Poincaré map. Using (3.30), we define

$$\underline{y}_{0,j} = \underline{y}_0(x_{\mathrm{f},j}, \overline{y}_{0,j}) = \overline{y}_{0,j} \left(\frac{1 - x_{\mathrm{f},j}}{1 - x_\star}\right)^{\frac{1-x_\star}{\epsilon}} e^{-\frac{x_\star - x_{\mathrm{f},j}}{\epsilon}}. \tag{3.48}$$

We can then iteratively define the time-forward Poincaré map on the y nullcline via

$$\overline{y}_{0,1} \to \underline{y}_{0,1} \to \overline{y}_{0,2} \to \underline{y}_{0,2} \to \overline{y}_{0,3} \to \underline{y}_{0,3} \to \cdots. \tag{3.49}$$

3.2. Improved matching including the y-axis boundary layer solution. We conclude our analysis with a second matching that includes the boundary layer solution along the y-axis, $\overset{\mathrm{yb}}{X}_0(y)$, (2.8), which contributes logarithmic terms similar to those provided by the corner solution (2.28) that facilitated our previous matching in (3.13). For biologically relevant parameters, this new matching improves significantly upon our formulae for $\overleftarrow{X}$, (3.23), and $\overrightarrow{X}$, (3.42).

Having a boundary layer along the y-axis is sensible only for trajectories that approach the y-axis. Consequently, when studying this layer, unlike previously (subsection 3.1), we are now assuming implicitly that $x_{\mathrm{f}} = \mathcal{O}(\epsilon)$ (since $x_{\mathrm{f}} < \underline{x}$ and no trajectory gets closer than $\underline{x}$ to the y-axis). In particular, since

$$\begin{aligned} x_{\mathrm{f}} &= -x_\star W_0\left(\mathscr{E}\left(-\frac{x_{\mathrm{i}}}{x_\star}\right) e^{-y_{\mathrm{i}}/x_\star}\right) = -\frac{1}{\mathcal{R}_0} W_0(\mathscr{E}(-\mathcal{R}_0 x_{\mathrm{i}}) e^{-\mathcal{R}_0 y_{\mathrm{i}}}) \\ &= x_{\mathrm{i}} e^{-\mathcal{R}_0(x_{\mathrm{i}} + y_{\mathrm{i}})} + \mathcal{O}(\mathcal{R}_0 x_{\mathrm{i}}^2 e^{-2\mathcal{R}_0(x_{\mathrm{i}} + y_{\mathrm{i}})}), \end{aligned} \tag{3.50}$$

and $x_{\mathrm{i}} + y_{\mathrm{i}} \leq 1$, we are implicitly assuming that $e^{-\mathcal{R}_0} = \mathcal{O}(\epsilon)$ or, equivalently, $\mathcal{R}_0 = \mathcal{O}(\ln \epsilon^{-1})$. For the diseases listed in Table 1, $\mathcal{R}_0 / \ln \epsilon^{-1}$ ranges from $\simeq 0.17$ (for pneumonic plague and influenza) to $\simeq 1.7$ (for measles and pertussis), suggesting it is not unreasonable to assume $\mathcal{R}_0 / \ln \epsilon^{-1} = \mathcal{O}(1)$. In Figure 4, $\mathcal{R}_0 / \ln \epsilon^{-1} \simeq 0.38$ in the top panels and $\simeq 1.7$ in the bottom panels.

As with our original matching (subsection 3.1), we use the outer solution expressed as a function of y, $\overset{\mathrm{out}}{X}{}^i_0(y)$ (3.6), and since we are matching in the left half-plane ($x \leq x_\star$), we set $i = 0$. Matching $\overset{\mathrm{out}}{X}{}^0_0(y)$ with the y-axis boundary layer solution $\overset{\mathrm{yb}}{X}_0(y)$ (2.8) is uncharacteristically simple: the two are of different asymptotic orders ($\mathcal{O}(1)$ and $\mathcal{O}(\epsilon)$), and the solutions have no overlap. The matched solution is thus their sum, with the constant $\overset{\mathrm{yb}}{C}_0$ as yet undetermined.

We set

$$\overset{\mathrm{yb}}{C}_0 = -E_1\left(\frac{\overline{y}_0}{x_\star}\right) \tag{3.51}$$

so that $\overset{yb}{X}_0(y)$ vanishes when evaluated at $(x_\star, \overline{y}_0)$ and consequently the sum $\overset{out}{X}_0^0(y) + \overset{yb}{X}_0(y)$ agrees at $(x_\star, \overline{y}_0)$ with $\overset{out}{X}_0^{-1}(y)$ (3.6), the corresponding focal approximation in the right half-plane ($x \geq x_\star$). Thus, $\overset{yb}{X}_0(y)$ becomes

$$\overset{yb}{X}_0(y) = \frac{\epsilon}{x_\star} e^{-y/x_\star} \left(E_1\left(\frac{y}{x_\star}\right) - E_1\left(\frac{\overline{y}_0}{x_\star}\right)\right). \tag{3.52}$$

With the choice (3.51) for $\overset{yb}{C}_0$, the sum

$$\begin{aligned} X_{\rm in}(y;\epsilon) &:= \overset{out}{X}_0^0(y) + \overset{yb}{X}_0(y) \\ &= -x_\star W_0\left(\mathscr{E}\left(-\frac{x_{\rm i}}{x_\star}\right) e^{(y-y_{\rm i})/x_\star}\right) + \epsilon \frac{e^{y/x_\star}}{x_\star}\left(E_1\left(\frac{y}{x_\star}\right) - E_1\left(\frac{\overline{y}_0}{x_\star}\right)\right) \end{aligned} \tag{3.53}$$

is a very good approximation to the trajectory, except in the x-axis boundary layer. Elsewhere [25], we use (3.53) to approximate the fraction susceptible at the point of entry into the set $\{(x,y) : y \leq y_\star\}$ (hence "in").

We next match with the inner solution expressed as a function of y, $\overset{xb}{X}_0^{-1}(y)$ (2.44) (now the $i = -1$ branch gives the solution with $x \leq x_\star$), for which we obtained the asymptotic expansion for $y = \eta y_\eta$ previously, (3.19).

To expand the matched outer and y-axis boundary layer solutions (3.53), we introduce the *complementary exponential integral* [23, 6.2.4],

$$\mathrm{Ein}(z) = \int_0^z \frac{1 - e^{-u}}{u}\,\mathrm{d}u, \tag{3.54}$$

an entire function that satisfies $\mathrm{Ein}(z) = z + \mathcal{O}(z^2)$ and

$$E_1(z) = \mathrm{Ein}(z) - \ln z - \gamma, \tag{3.55}$$

where $\gamma \simeq 0.57721$ is the Euler–Mascheroni constant [23, 5.9.18] (not the recovery rate in the SIR model (1.1)). Using (3.55), (3.53) becomes

$$X_{\rm in}(y;\epsilon) = x_{\rm f} + \eta\left(\frac{x_{\rm f}}{x_\star - x_{\rm f}}\right) y_\eta + \epsilon \ln \eta^{-1} \frac{1}{x_\star} + \epsilon \frac{1}{x_\star}\left(\ln \overline{y}_0 - \ln y_\eta + \mathrm{Ein}\left(\frac{\overline{y}_0}{x_\star}\right)\right) + \mathcal{O}(\epsilon\eta). \tag{3.56}$$

Comparing this expression with the asymptotic series expansion for the x-axis boundary layer solution (3.19), we see that the coefficient of $\ln y_\eta$ appears to be different in the two expansions ($\frac{\epsilon}{x_\star}$ in (3.56) versus $\epsilon\frac{1-x_{\rm f}}{x_\star - x_{\rm f}}$ in (3.19)). This apparent difference is a consequence of the assumption implicit throughout this section that $x_{\rm f} = \mathcal{O}(\epsilon)$, which implies that $\epsilon\frac{1-x_{\rm f}}{x_\star - x_{\rm f}} = \frac{\epsilon}{x_\star} + \mathcal{O}(\epsilon^2)$, so the two coefficients are in fact *asymptotically* equal. With this in mind, we see that, as in the original matching,

$$c_0^{\phi} = x_{\mathrm{f}}, \tag{3.57}$$

from which we obtain C_0^{ϕ} via (3.17), whereas now

$$C_1^{\phi} = \ln \overline{y}_{_0} - \mathrm{Ein}\left(\frac{\overline{y}_{_0}}{x_{_\star}}\right). \tag{3.58}$$

Substituting c_0^{ϕ} and C_1^{ϕ} into (2.44) yields

$$\overset{\text{xb}}{X}{}_0^{i}(y) = 1 + (1 - x_{_\star})\, W_i\left(\mathscr{E}\left(-\frac{1-x_{\mathrm{f}}}{1-x_{_\star}}\right)\left(\frac{\overline{y}_{_0}}{y}\right)^{\frac{\epsilon}{1-x_{_\star}}} e^{-\frac{\epsilon}{1-x_{_\star}}\mathrm{Ein}(\overline{y}_{_0}/x_{_\star})}\right). \tag{3.59}$$

This expression differs from the matched boundary layer solution $\overset{\text{xb}}{X}{}_0^{-1}(y)$ (3.26) by an additional factor

$$e^{-\frac{\epsilon}{1-x_{_\star}}\mathrm{Ein}(\overline{y}_{_0}/x_{_\star})} = 1 - \frac{\epsilon}{1-x_{_\star}}\mathrm{Ein}\left(\frac{\overline{y}_{_0}}{x_{_\star}}\right) + \mathcal{O}(\epsilon^2), \tag{3.60}$$

which multiplies the argument of the W-function, giving an $\mathcal{O}(\epsilon)$ refinement to $\overset{\text{xb}}{X}{}_0^{-1}(y)$.

Summing the outer and two inner solutions and subtracting the common overlap yields a solution uniformly valid to the left of $x = x_{_\star}$,

$$\overleftarrow{X}(y;\epsilon) = \overset{\text{out}}{X}{}_0^{0}(y) + \overset{\text{yb}}{X}{}_0(y) + \overset{\text{xb}}{X}{}_0^{-1}(y) - x_{\mathrm{f}} + \frac{\epsilon}{x_{_\star}}\left(\ln\left(\frac{y}{\overline{y}_{_0}}\right) + \mathrm{Ein}\left(\frac{\overline{y}_{_0}}{x_{_\star}}\right)\right). \tag{3.61}$$

This solution can be extended the right half-plane ($x \geq x_{_\star}$) using the $i = 0$ branch of (2.44), with c_0^{ϕ}, C_0^{ϕ}, and C_1^{ϕ} as determined above. The matching to the second epidemic wave then proceeds identically to subsection 3.1.3 (except that the argument of the inner solution now has the additional factor $e^{-\frac{\epsilon}{1-x_{_\star}}\mathrm{Ein}(\overline{y}_{_0}/x_{_\star})}$), resulting in

$$\overrightarrow{X}(y;\epsilon) = \overset{\text{out}}{X}{}_0^{-1}(y) + \overset{\text{xb}}{X}{}_0^{0}(y) - x_{\mathrm{i},2}. \tag{3.62}$$

We summarize these results in Table 3 and compare them to the numerically evaluated trajectories in Figure 4(b).

Subsequent epidemic waves. Just as before (subsection 3.1.4), these solutions can be extended to subsequent epidemic waves, replacing $\overline{y}_{_0}$, x_{f}, and $x_{\mathrm{i},2}$ by $\overline{y}_{_{0,j}}$, $x_{\mathrm{f},j}$, and $x_{\mathrm{i},j+1}$ defined using the iterative scheme in (3.46a)–(3.46c).

4. Discussion. Nonlinear differential equations can rarely be solved exactly. Creative analyses leading to approximate analytical solutions were once the only way to study nonlinear systems (see [24, pp. 201–204] for a very concise history), but interest in such approximations has diminished as computers have become more powerful and software for efficient and accurate numerical solution of differential equations has become so easily accessible. However, closed-form analytical expressions can often lead to valuable insights and can facilitate further analyses that would be impossible or exceedingly challenging to conduct numerically.

We have derived new, fully analytical approximations for the phase plane dynamics of the SIR model with vital dynamics. In Table 2, we list our expressions for key epidemiological quantities, including peaks and troughs of the susceptible and infectious proportions of the host population. We present a closed-form analytical

approximation to the Poincaré map for the SIR model in subsection 3.1.4. A highly accurate approximation to the susceptible proportion as the trajectory enters the x-axis boundary layer is given in (3.53) and is a critical ingredient in a stochastic disease persistence analysis that we present elsewhere [25].

Our approach has involved matching asymptotic expansions across branch cuts of a special function (the Lambert W function, subsection 2.5). To our knowledge, this is the first example of asymptotic matching across branch cuts.

We have considered only the standard SIR model, but the techniques we have presented can be adapted to other compartmental ODE models. The essential ingredients are a biologically plausible small parameter (e.g., ε (1.3) or ϵ (1.6), as considered here, or the rate of waning of immunity after infection or vaccination) and an analytically tractable outer solution (e.g., the KM solution to the SIR model without vital dynamics (3.5), as used here, or solutions of other simple models with nonlinear incidence rates [28]). We will explore such possibilities in further work.

Appendix A. The failure of direct series in the x-axis boundary layer. Knowing that the equilibrium infective frequency $y_\star$ is $\mathcal{O}(\epsilon)$ (1.8b), we might plausibly posit a boundary layer solution

$$\overset{x\mathrm{b}}{Y}(x;\epsilon) = \epsilon\Upsilon(x;\epsilon)\,, \tag{A.1}$$

where $\Upsilon = \mathcal{O}(1)$. Substituting $\epsilon\Upsilon$ for Y in (1.10) yields

$$\epsilon((1-x) - x\Upsilon(x;\epsilon))\frac{\mathrm{d}\Upsilon}{\mathrm{d}x} = (x - x_\star)\Upsilon(x;\epsilon)\,. \tag{A.2}$$

Searching for an asymptotic series solution in powers of ϵ,

$$\Upsilon(x;\epsilon) = \sum_{j=0}^{\infty}\Upsilon_j(x)\epsilon^j\,, \tag{A.3}$$

and collecting terms of common order ϵ^j yields, for $j = 0$,

$$0 = (x - x_\star)\Upsilon_0(x)\,, \tag{A.4a}$$

which implies that $\Upsilon_0(x) \equiv 0$. Now, suppose that $\Upsilon_0(x) \equiv \cdots \equiv \Upsilon_{j-1}(x) \equiv 0$; then, for $j \geq 1$, collecting terms of order ϵ^j in (A.2) yields

$$0 = (x - x_\star)\Upsilon_j(x)\,. \tag{A.4b}$$

By induction, it follows that $\Upsilon_j(x) \equiv 0$ for all j, and hence that $\overset{x\mathrm{b}}{Y}(x;\epsilon) \equiv 0$, which is a contradiction. We must conclude that our assumption in (A.3) that $\Upsilon(x;\epsilon)$ can be expanded in a series of powers of ϵ is incorrect.

Appendix B. Summary table of matching constants. Table 4 lists the matching constants.

TABLE 4

Matching constants for initial conditions $(x_{\rm i}, y_{\rm i})$. *Subscripts* (0, ln, 1) *refer to asymptotic orders, oversets* (out, cor, *y*b) *refer to regions where the associated asymptotic expressions are valid, and the superscript* (ϕ) *refers to expansion of the auxiliary function* $\phi(x;\epsilon)$ (2.10). *Left and right indicate constants appearing in the left and right corner solutions, while* 2*nd indicates constants for the second epidemic wave. See Table* 2 *for* $x_\star$, $x_{\rm f}$, $\overline{y}_0$, *and* $x_{\rm i,2}$ *expressed in terms of* $\mathcal{R}_0$ *and* ϵ. *The final expressions with these values for the matching constants are listed in Table* 3.

Constant	Expression	Equations
$\overset{\rm out}{C}_0$	$y_{\rm i} + x_{\rm i} - x_\star \ln x_{\rm i}$	(2.3), (2.43), (3.4)
$\overset{\rm cor}{C}_0$ (left)	$x_{\rm f}$	(2.21), (2.28), (3.15)
$\overset{\rm cor}{C}_{\ln}$ (left)	$\frac{1-x_{\rm f}}{x_\star - x_{\rm f}}$	(2.28), (3.15)
$\overset{\rm cor}{C}_1$ (left)	$\frac{1-x_{\rm f}}{x_\star - x_{\rm f}} \ln \overline{y}_0$	(2.28), (3.20), (3.25)
c_0^ϕ	$x_{\rm f}$	(3.20)
C_0^ϕ	$x_{\rm f} - (1-x_\star)\ln(1-x_{\rm f})$	(2.15), (2.18), (2.44), (3.17), (3.20)
C_1^ϕ	$\ln \overline{y}_0$	(2.16), (2.18), (2.44), (3.25)
$\overset{\rm cor}{C}_0$ (right)	$x_{\rm i,2}$	(2.21), (2.28), (3.35)
$\overset{\rm cor}{C}_{\ln}$ (right)	$\frac{1-x_{\rm i,2}}{x_\star - x_{\rm i,2}}$	(2.28), (3.35)
$\overset{\rm cor}{C}_1$ (right)	$\frac{1-x_{\rm i,2}}{x_\star - x_{\rm i,2}} \ln \overline{y}_0$	(2.28), (3.35)
$\overset{\rm out}{C}_0$ (2nd)	$x_{\rm i,2}$	(2.3), (2.43)
$\overset{\rm out}{c}_0$ (2nd)	$x_{\rm i,2} - x_\star \ln x_{\rm i,2}$	(3.37), (3.38), (3.40)
$\overset{y\rm b}{C}_0$	$-E_1(\frac{\overline{y}_0}{x_\star})$	(2.8), (3.51)
C_1^ϕ (y-axis matching)	$\ln \overline{y}_0 - \mathrm{Ein}(\frac{\overline{y}_0}{x_\star})$	(2.16), (2.18), (2.44), (3.58)

Acknowledgments. We are grateful to Emma Coates for carefully reading the manuscript and providing helpful comments.

REFERENCES

[1] J. D. ANDERSON, *Ludwig Prandtl's boundary layer*, Phys. Today, 58 (2005), pp. 42–48.
[2] R. M. ANDERSON AND R. M. MAY, *Infectious Diseases of Humans: Dynamics and Control*, Oxford University Press, Oxford, UK, 1991.
[3] N. BACAËR, *McKendrick and Kermack on epidemic modelling* (1926-1927), in A Short History of Mathematical Population Dynamics, Springer, London, 2011, pp. 89–96.
[4] N. BACAËR, *The model of Kermack and McKendrick for the plague epidemic in Bombay and the type reproduction number with seasonality*, J. Math. Biol., 64 (2012), pp. 403–422.
[5] C. M. BENDER AND S. A. ORSZAG, *Advanced Mathematical Methods for Scientists and Engineers*, McGraw-Hill, New York, 1978.
[6] D. CHAMPREDON, J. DUSHOFF, AND D. J. D. EARN, *Equivalence of the Erlang-distributed SEIR epidemic model and the renewal equation*, SIAM J. Appl. Math., 78 (2018), pp. 3258–3278.
[7] R. M. CORLESS, G. H. GONNET, D. E. G. HARE, D. J. JEFFREY, AND D. E. KNUTH, *On the Lambert W function*, Adv. Comput. Math., 5 (1996), pp. 329–359.
[8] P. FLAJOLET AND R. SEDGEWICK, *Analytic Combinatorics*, Cambridge University Press, Cambridge, UK, 2009.
[9] R. GANI AND S. LEACH, *Epidemiologic determinants for modeling pneumonic plague outbreaks*, Emerg. Infect. Dis., 10 (2004), pp. 608–614.
[10] D. HE AND D. J. D. EARN, *Epidemiological effects of seasonal oscillations in birth rates*, Theor. Popul. Biol., 72 (2007), pp. 274–291.

[11] H. W. Hethcote, *Three basic epidemiological models*, in Applied Mathematical Ecology, S. A. Levin, T. G. Hallam, and L. J. Gross, eds., Springer, New York, 1989, pp. 119–144.
[12] T. D. Hollingsworth, R. M. Anderson, and C. Fraser, *HIV-1 transmission, by stage of infection*, J. Infect. Dis., 198 (2008), pp. 687–693.
[13] W. O. Kermack and A. G. McKendrick, *A contribution to the mathematical theory of epidemics*, Proc. A, 115 (1927), pp. 700–721.
[14] J. Kevorkian and J. D. Cole, *Multiple Scale and Singular Perturbation Methods*, Springer-Verlag, New York, 1996.
[15] O. Krylova, *Predicting Epidemiological Transitions in Infectious Disease Dynamics: Smallpox in Historic London* (1664-1930), Ph.D. thesis, McMaster University, Canada, 2011.
[16] O. Krylova and D. J. D. Earn, *Effects of the infectious period distribution on predicted transitions in childhood disease dynamics*, J. Roy. Soc. Interface, 10 (2013) 20130098.
[17] Z. Levine and D. J. D. Earn, *Face masking and COVID-19: Potential effects of variolation on transmission dynamics*, J. Roy. Soc. Interface, 19 (2022), 20210781.
[18] J. Ma and D. J. D. Earn, *Generality of the final size formula for an epidemic of a newly invading infectious disease*, Bull. Math. Biol., 68 (2006), pp. 679–702.
[19] A. G. McKendrick, *Applications of mathematics to medical problems*, Proc. Edinburgh Math. Soc., 13 (1926), pp. 98–130.
[20] C. E. Mills, J. M. Robins, and M. Lipsitch, *Transmissibility of* 1918 *pandemic influenza*, Nature, 432 (2004), pp. 904–906.
[21] A. A. Milne, *Winnie-the-Pooh*, Methuen, London, 1926.
[22] R. Olinky, A. Huppert, and L. Stone, *Seasonal dynamics and thresholds governing recurrent epidemics*, J. Math. Biol., 56 (2008), pp. 827–839.
[23] F. W. J. Olver, D. W. Lozier, R. F. Boisvert, and C. W. Clark, eds., *NIST Handbook of Mathematical Functions*, National Institute of Standards and Technology and Cambridge University Press, New York, 2010.
[24] R. E. O'Malley, Jr., *Singular Perturbation Methods for Ordinary Differential Equations*, Appl. Math. Sci. 89, Springer, New York, 1991.
[25] T. L. Parsons, B. M. Bolker, J. Dushoff, and D. J. D. Earn, *The probability of epidemic burnout in the stochastic SIR model with vital dynamics*, Proc. Natl. Acad. Sci. USA, 121 (2024), e2313708120.
[26] L. Stone, R. Olinky, and A. Huppert, *Seasonal dynamics of recurrent epidemics*, Nature, 446 (2007), pp. 533–536.
[27] O. A. van Herwaarden, *Stochastic epidemics: The probability of extinction of an infectious disease at the end of a major outbreak*, J. Math. Biol., 35 (1997), pp. 793–813.
[28] E. B. Wilson and J. Worcester, *The law of mass action in epidemiology*, Proc. Natl. Acad. Sci. USA, 31 (1945), pp. 24–34.
[29] Z. Y. Wong, C. M. Bui, A. A. Chughtai, and C. R. Macintyre, *A systematic review of early modelling studies of Ebola virus disease in West Africa*, Epidemiol. Infect., 145 (2017), pp. 1069–1094.